Diffusivity in asymmetric Yukawa ionic mixtures in dense plasmas

Tomorr Haxhimali, Robert E. Rudd, William H. Cabot, and Frank R. Graziani

Phys. Rev. E **90**, 023104 — Published 21 August 2014

DOI: 10.1103/PhysRevE.90.023104

Diffusivity in asymmetric Yukawa ionic mixtures in dense plasmas

Tomorr Haxhimali, Robert E. Rudd, William H. Cabot, and Frank R. Graziani
Lawrence Livermore National Laboratory,
Livermore, California 94550, USA

In this paper we present molecular dynamics (MD) calculations of the interdiffusion coefficient for asymmetric mixed plasma for thermodynamic conditions relevant to astrophysical and Inertial Confinement Fusion plasmas. Specifically, we consider mixtures of deuterium and argon at temperatures of 100-500 eV and a number density $\sim 10^{25}$ ions/cm^3. The motion of 30000-120000 ions is simulated in which the ions interact via the Yukawa (screened Coulomb) potential. The electric field of the electrons is included in this effective interaction; the electrons are not simulated explicitly. The species diffusivity is then calculated using the Green-Kubo approach using an integral of the interdiffusion current autocorrelation function, a quantity calculated in the equilibrium MD simulations. Our MD simulation results show that a widely used expression relating the interdiffusion coefficient with the concentration-weighted sum of self-diffusion coefficients, over-estimates the interdiffusion coefficient. We argue that this effect due to cross-correlation terms in velocities is characteristic of asymmetric mixed plasmas. Comparison of the MD results with predictions of kinetic theories also show a discrepancy with MD giving effectively a larger Coulomb logarithm.

PACS numbers: 52.25.Fi,52.27.Gr,52.29.Hq

I. INTRODUCTION

Transport processes in plasmas and warm dense matter are the subject of increasing interest [1–7]. These transport processes have long been treated in the framework of kinetic theories [1]. Chapman-Enskog theory predicts values for the transport coefficients, typically using a binary collision operator. For bare Coulomb charges, the resulting scattering integrals include a Coulomb logarithm in which long-range screening and short-range quantum effects (or the classical turning point for repulsive charges) cut off the otherwise divergent integral. These calculations rely on weak coupling, and as the coupling increases, the accuracy of the predicted transport coefficient declines, often phrased as uncertainty in the Coulomb logarithm. As computer power has increased, it has become practical to calculate plasma transport coefficients using molecular dynamics (MD) [2–4, 7–11]. MD does not rely approximations based on weak coupling, binary collisions, or small-angle scattering. In fact, MD performs better by some measures in strongly coupled plasmas, and as computer power increases further, MD may be extended up to new regimes of weak coupling [12, 13]. Most of the MD work has focused on simulations of plasmas with at most one ionic species, with or without explicit electrons. Here we use MD to simulate transport processes in an asymmetric plasma mixture, a plasma with two ionic species with quite different charges and masses. We focus on the species diffusivity in a case where the ion-ion coupling of one species is strong while that of the other species is weak to moderate. Various predictions for species diffusivity have been made based on kinetic theories [1, 10, 14, 15] and by using effective couplings in models derived from single species self-diffusivity [4–6]. Some comparisons have been made [16], but the question of the accuracy of the kinetic and effective theories largely remains open. We assess that question here.

The species diffusivity is important in mixing processes. Mixing involves both advective stirring and mixing at the atomic level due to the species diffusivity. Typically, the advection is the principal mechanism for mixing material over longer length and time scales, but the species diffusivity provides an important mechanism for irreversibility and may dominate at short time scales. For brevity, throughout the remainder of this Article we refer to species diffusivity simply as diffusivity. Within plasma physics, diffusion plays an important role in some well-known systems. It is key to the purification of white dwarf atmospheres through the gravitational sedimentation of heavy elements such as ^{22}Ne [17–19]. Diffusion can also have an effect in inertial confinement fusion (ICF), since mixing can degrade the fuel both in conventional hot spot ignition [20] and in double shell ignition [21]. Other systems exhibit diffusion of particles interacting through screened Coulomb interactions, such as dust particles in plasmas and colloidal particles suspended in electrolyte [22–25]. Diffusion in these systems spans a large range of regimes. ICF plasmas are dense. The fuel starts cold and at solid density $\sim$1 g/cm^3, is rapidly compressed to warm dense matter conditions, and ultimately while burning should be at temperatures $\sim$1 keV and densities of $\sim$1000 g/cm^3 [20]. White dwarfs have temperatures of 20 to 1000 eV and a broad range of densities. Diffusion is of interest in plasmas that are weakly coupled (white dwarf) to strongly coupled (early phase ICF). Understanding diffusion across this large range of conditions is a challenge, and there are no direct experimental measurements of diffusion in dense plasmas.

Diffusivity determines the relationship between the mean-squared displacement $|\Delta\mathbf{r}|^2$ of a diffusing particle to the time for that diffusion, Δt: $D = |\Delta\mathbf{r}|^2/(6\Delta t)$. To be precise, this is the self-diffusivity. Dimensionally, it is the product of a characteristic velocity and a scattering

length, so a first estimate of the diffusivity of a rarefied plasma is $D \approx v_{th} l_{mfp}$, where v_{th} is the thermal velocity and l_{mfp} is the mean free path. The more precise Chapman-Cowling formula [1] is:

$$D = \frac{\pi}{4} \frac{v_{th}\, r_{WS}}{\Gamma_{12}^2 \ln \Lambda} \tag{1}$$

$$\Gamma_{12} = Z_1 Z_2 \Gamma, \tag{2}$$

where Z_i is the charge on ion species i, e is the electron charge magnitude, $v_{th} = \sqrt{8 k_B T / \pi m_{red}}$, and $\Gamma \equiv e^2/(4\pi\epsilon_0\, r_{WS}\, k_B T)$. T is the temperature and k_B is the Boltzmann constant. The Wigner-Seitz radius is $r_{WS} = (4\pi n/3)^{-1/3}$, n is the total ion number density and m_{red} is the reduced mass of the two ions involved in the binary scattering events. Here $\ln\Lambda$ is the Coulomb logarithm. This diffusivity formula due to Chapman and Cowling [1] is for the Maxwell-Stefan diffusivity; i.e., the interdiffusivity without the thermodynamic factor, a factor that accounts for non-ideal mixing contributions to the free energy. Other kinetic model results based on screened Coulomb interactions from Paquette et al. [14] and Daligault [4] are also for the Maxwell-Stefan diffusivity.

The first studies of diffusion using MD were for a one component plasma (OCP), in which the ions interacted via the bare Coulomb force [26]. These studies focused on the velocity autocorrelation function and the self-diffusivity, i.e., the diffusivity of a tracer particle in the single-species plasma. The calculated diffusivity at strong coupling was greater than predicted by the Chapman-Cowling formula. The bare Coulomb interaction effectively assumes that the electrons are just a uniform, neutralizing background. Subsequent calculations have been done using a screened Coulomb (Yukawa) interaction and other effective interactions between the ions, relaxing the uniform background assumption [3, 5]. Here, too, the calculated self-diffusivity was greater than predicted by the Chapman-Cowling formula.

In a few cases MD simulations of interdiffusion in binary ionic mixtures have been reported [9, 10, 16]. These simulations have two ionic species and the ions interact via the bare Coulomb force. Here the Maxwell-Stefan diffusivity was calculated and multiplied by the thermodynamic factor for ideal, ambipolar electrons to get the interdiffusivity (mutual diffusivity). Bastea found that the MD-derived Maxwell-Stefan diffusivity for a D-Au mixture agreed well with the Paquette diffusivity [16]. Daligault proposed an interdiffusivity model based on his self-diffusivity calculations, using an effective coupling for the mixture and a Darken rule for combining self-diffusivities into an interdiffusivity [4]. There have also been some studies of diffusion using orbital-free density function theory and quantum molecular dynamics [27–29]. These approaches solve for the electron densities and the forces arising from them explicitly using approximate formulations of quantum mechanics. They hold the promise of more accurate forces, but at greatly increased computational cost which impacts the ability to collect good statistics and have simulation boxes larger than the ionic mean free path. Despite this body of work, important questions remain unresolved: Is diffusion in asymmetric binary plasma mixtures described well by kinetic models like the Chapman-Cowling formula when one component is strongly coupled? In those plasmas is it possible to relate the interdiffusivity to the computationally facile self-diffusivity? How important are cross-correlation effects in asymmetric plasmas? We address some of those questions here.

The text is organized as follows. In Section II we briefly describe the multispecies plasmas followed by a review of the hydrodynamics equations, and as a continuation in Section III we present the Green-Kubo approach that is used in this work to extract diffusion coefficient. In Section IV the methodology of the work and details of MD are discussed, and in Section V results and comparison with kinetic theories are presented. Finally, we conclude with a summary in Section VI.

II. FORMALISM

A. Description of Mixed Plasma

We start our discussion with a review of the parameters needed to describe mixed plasmas. We assume a mixture of the ion species $i = 1, 2, ...$ with mass and ionization A_i and Z_i^*, respectively. The total number density of ions is given by $n = \sum_i n_i$, where n_i is the number density of the ions of species i. The Wigner-Seitz radius of the system is given by $r_{WS} = (\frac{4}{3}\pi n)^{-1/3}$. The strength of the ion-ion Coulomb interaction–ratio of potential to kinetic energy– for species i is characterized by the coupling parameter:

$$\Gamma_i = \frac{(Z_i^* e)^2}{4\pi\epsilon_0 r_i k_B T} = (Z_i^*)^{5/3} \langle Z^* \rangle^{1/3} \Gamma, \tag{3}$$

where $r_i = \frac{(Z_i^*)^{1/3}}{\langle Z^* \rangle^{1/3}} r_{WS}$ is the ion sphere radius introduced by Salpeter [30]. In a multicomponent mixed plasma it is useful to introduce an effective coupling [4, 16, 31–33]:

$$\Gamma_{\text{eff}} = \sum_i X_i \Gamma_i = \langle (Z^*)^{5/3} \rangle \langle Z^* \rangle^{1/3} \Gamma. \tag{4}$$

In Eqs. (3) and (4) we use the definition for the angular brackets $\langle \cdots \rangle$ as a number-weighted average of a parameter Ψ in a mixture of the type $\langle \Psi \rangle = \sum_i \Psi_i X_i$ where $X_i = n_i/n$ is the mole fraction of species i. For a plasma mixture the effective coupling will change with the mole fraction as well as temperature and density. In Fig. 1 we plot Γ_{eff} in a mixture of D and Ar ions as a function of composition and temperature, across the range of conditions studied in this Article. The interspecies coupling parameter Γ_{12} in Eq. (1) on the other hand is independent of the composition mole fraction and cannot effectively describe the mixture.

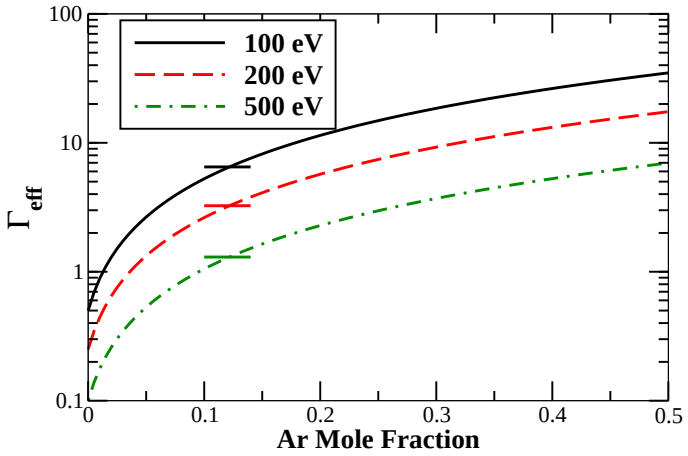

FIG. 1. (Color online) Effective coupling $\Gamma_{\rm eff}$ using relation (4) as a function of Ar mole fraction in a D-Ar ionic mixture at $T = 100$, 200 and 500 eV density 10^{25} ion/cm^3 and ionization $Z^*_{\rm D} = 1$ and $Z^*_{\rm Ar} = 13$. As a reference the values of Γ_{12} are 6.5, 3.25 and 1.3 for $T = 100$, 200 and 500 eV, respectively. These are represented with the short horizontal lines around the value of the mole fraction where $\Gamma_{12} = \Gamma_{eff}$.

The ionic mixture is immersed in a neutralizing background of free electrons whose state is determined by the electron number density n_e and temperature T. From the global charge neutrality of the mixture the number density of the electrons is given by:

$$n_e = \langle Z^* \rangle \, n. \tag{5}$$

In charged fluids the electrons interact not only with their immediate neighbors but with all the other electrons in the system, therefore their motion cannot be decoupled from one another. As a consequence plasmas exhibit a strong collective behavior in the long wavelength limit, $k \to 0$, where the Fourier transform of the Coulomb potential, $e^2/\epsilon_0 k$, diverges. A manifestation of this behavior is the polarizability of the electrons which rearrange themselves around the ions so that the plasma remains locally neutral. This rearrangement leads to an effective inter-ion potential that decays much faster than $1/r$ at large distances. In this work we use the Yukawa potential to describe the ionic effective potential. It captures the electron polarizability in a linear response regime [34, 35]. Several recent articles [36, 37] have verified its validity in warm and hot dense matter regimes, and it is expected to provide an accurate description of the 100 eV and hotter plasmas studied here. Polarizable BIM models [38–40] have been developed for binary mixed plasmas based on a similar motivation. We give more details for the ion-ion effective potential in the Methodology Section (IV).

Defining parameters that describe the electron fluid is integral to the description of ionic mixture. It is convenient to introduce the dimensionless length parameter $r_s = r_e/a_0$, where $r_e = (\frac{4}{3}\pi n_e)^{-1/3}$ and a_0 is the Bohr radius. As T and n_e change, the electrons span different levels of the degeneracy which can be characterized by the dimensionless parameter $\Theta \equiv k_B T/E_F$ [41, 42], where $E_F \equiv \frac{\hbar^2}{2m_e}\left(3\pi^2 n_e\right)^{2/3}$ is the Fermi energy and m_e the mass of the electron. In the high density and degenerate plasma limit, i.e. $r_s \to 0$ and $\Theta \to 0$ respectively, the electrons form a rigid neutralizing background.

For fully to partially degenerate electrons, quantum effects are important. To extend the coupling definition to the quantum regime, we need to account for the fact that electrons do not get arbitrary close to each other. Here Γ_e is taken to be the ratio of the potential energy to the Fermi energy $\Gamma_e = e^2/\left(4\pi\epsilon_0\, r_e\, E_f\right)$, whereas for non-degenerate electrons $\Gamma_e = e^2/\left(4\pi\epsilon_0\, r_e\, k_B T\right)$. For partially degenerate case an interpolation form between the two extremes may be employed [43]:

$$\Gamma_e = \frac{1}{4\pi\epsilon_0}\frac{e^2}{r_e\sqrt{(k_B T)^2 + E_f^2}}. \tag{6}$$

The effective coupling for the D-Ar plasma mixtures studied here ranges from ∼0.1 to ∼35, depending on the temperature and the Ar mole fraction, as shown in Fig. 1. They span a range of moderate couplings. In Fig. 2 we plot the degeneracy parameter Θ as a function of the Ar mole fraction for the same temperatures with $n = 10^{25}$ ion/cm^3. The 100 eV and 200 eV plasmas have $\Theta < 1$, apart from the 200 eV nearly pure D plasmas ($X < 0.025$). $\Theta = 0$ corresponds to a fully degenerate plasma, so the plasmas studied here are moderately degenerate. For the 500 eV plasmas, Θ ranges from 0.8 to ∼3. In the same figure we plot the so called warm dense matter (WDM) parameter $\mathcal{W} = S(\Gamma_e)S(\Theta)$, introduced by Murillo [43], with $S(x) = 2/\left(x + x^{-1}\right)$ a function that is symmetric under $x \to 1/x$ and peaks at unity. These

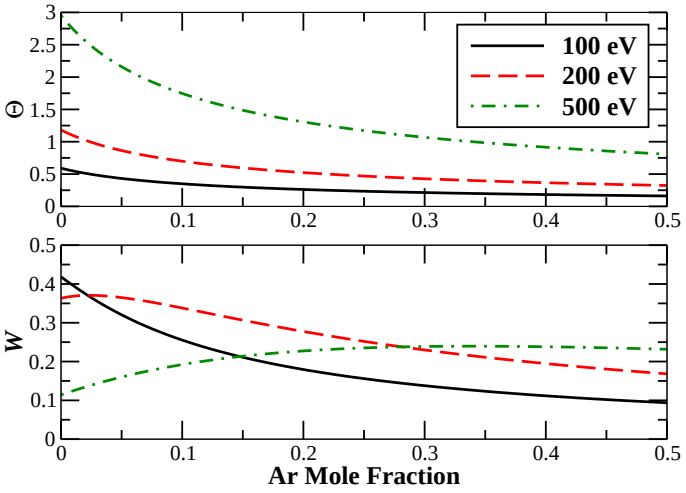

FIG. 2. (Color online) Electron degeneracy Θ and warm dense matter parameter $\mathcal{W}$ [43] as a function of Ar mole fraction in a D-Ar ionic mixture at $T = 100$, 200 and 500 eV density 10^{25} ion/cm^3 and ionization $Z^*_{\rm D} = 1$ and $Z^*_{\rm Ar} = 13$.

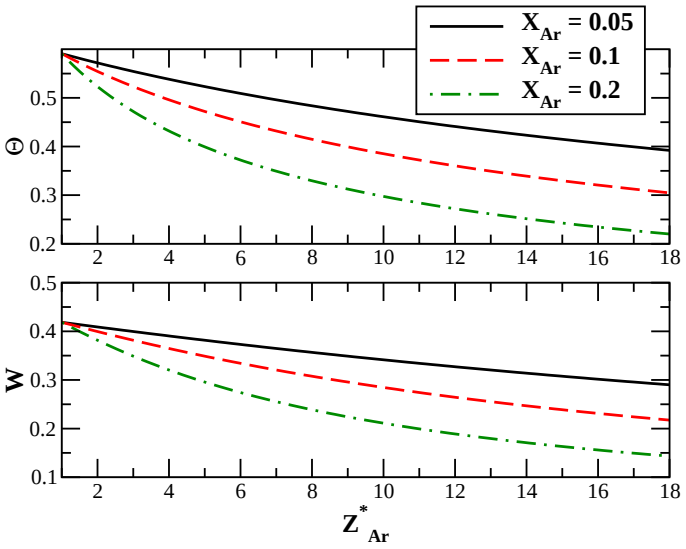

FIG. 3. (Color online) Electron degeneracy Θ and warm dense matter parameter $\mathcal{W}$ [43] as a function of Ar ionization in a D-Ar ionic mixture at $T = 100$ eV, density 10^{25} ion/cm^3 and Ar mole composition $X_{Ar} = 0.05, 0.1$ and 0.2. The ionization of D was kept fixed at $Z^*_{\rm D} = 1$.

plasmas are approaching warm dense matter ($\mathcal{W} = 1$). In Fig. 3 we plot the degeneracy parameter Θ as well as $\mathcal{W}$ as a function of Ar ionization for the same mixture at 100 eV, for three values of Ar mole fraction. From an average atom calculation (Section V B) we expect the value of $Z^*_{Ar} \sim 10$. We can deduce from Fig. 3 that the value of Θ will be in the range $0.3-0.5$ for these mixtures.

B. Hydrodynamics

In this Section we review the mixing in neutral and ionic fluids in the hydrodynamic limit. In this limit the local properties of the fluid vary slowly on microscopic length and time scales; as such the fluid is described by the equations of macroscopic fluid mechanics [44, 45]. The conservation laws and dissipative fluxes are described by the Navier-Stokes equations for multicomponent fluids. The complete set of these equations is complicated and given in standard texts [46, 47]. Here we consider the binary mixture case and write only equations that are relevant to the diffusion. The treatment of a binary mixture can be extended to a multicomponent mixture [48]. The conservation equations for mass and momentum and the equation for the species flux are:

$$\frac{\mathfrak{D}\rho}{\mathfrak{D}t} = -\rho\nabla\cdot\mathbf{v}, \tag{7}$$

$$\rho\frac{\mathfrak{D}c}{\mathfrak{D}t} = -\nabla\cdot\mathbf{j^c} + r, \tag{8}$$

$$\rho\frac{\mathfrak{D}\mathbf{v}}{\mathfrak{D}t} = -\nabla P - \nabla\cdot\tau + \rho\mathbf{g}, \tag{9}$$

where $\mathfrak{D}/\mathfrak{D}t = \partial_t + \mathbf{v}\cdot\nabla$ is the comoving derivative. In this set of equations $\rho(\mathbf{r})$ is mass density and $c(\mathbf{r})$ is the mass fraction of species 1. The equations are written for a binary mixture so the indices in the previous definition have been dropped. The center-of-mass velocity $\mathbf{v}(\mathbf{r})$ is given by $\rho\mathbf{v} = \rho_1\mathbf{v}_1 + \rho_2\mathbf{v}_2$ with ρ_i and $\mathbf{v_i}$ being the mass density and mean velocity of species i. The inter-diffusion current, $\mathbf{j}^c = \rho_1(\mathbf{v_1} - \mathbf{v}) = \rho c(1-c)(\mathbf{v_1} - \mathbf{v_2})$, is modeled. Here τ_{ij} is the energy-momentum tensor related to the stress tensor σ_{ij} by $\tau_{ij} = \rho v_i v_j - \sigma_{ij}$. The rate of production of mass of one species due to chemical reaction or fusion events in dense plasmas, which will be ignored in this study, is denoted by r; $\mathbf{g}$ is the gravitational acceleration. The other fields are the internal energy per unit mass E, pressure $P = -\frac{1}{3}\sigma_{ii}$, and temperature T.

The hydrodynamic variables obey phenomenological equations relating species mass and heat fluxes (or currents) with gradients of local variables. More generally we relate the mass fluxes to a driving force proportional to the gradient of the difference chemical potentials per unit mass μ of the two components:

$$\mu = \frac{\mu_1}{m_1} - \frac{\mu_2}{m_2}, \tag{10}$$

with μ_i and m_i the chemical potential and mass of species i, respectively. In addition, there is a temperature gradient term from collisional heat exchange (the Soret effect) [49]. The gradient in μ can be cast in terms of gradients of different local variables. For a neutral binary mixture $\nabla\mu$ can be expressed as [44]:

$$\nabla\mu(\mathbf{r},t) = \left(\frac{\partial\mu}{\partial c}\right)_{P,T}\nabla c(\mathbf{r},t) + \left(\frac{\partial\mu}{\partial P}\right)_{T,c}\nabla P(\mathbf{r},t) + \left(\frac{\partial\mu}{\partial T}\right)_{P,c}\nabla T(\mathbf{r},t). \tag{11}$$

The temperature gradient term from the chemical potential is often combined with the Soret term. In the above linear response approach, the mass flux $\mathbf{j}^c$ can be written as:

$$\mathbf{j}^c = -\rho D_{12}\left[\nabla c + (k_T/T)\nabla T + (k_P/P)\nabla P\right], \tag{12}$$

where D_{12} is the interdiffusivity, $k_T D_{12}$ the thermal diffusion coefficient and $k_P D_{12}$ the barodiffusion coefficient. In isothermal-isobaric conditions, Eq. (12) reduces to $\mathbf{j}^c = -\rho D_{12}\nabla c$, which combined with Eq. (8) gives the familiar Fick's law for diffusion in mixtures.

For ionic mixtures, which include plasmas, the situation is a bit more complicated since compositional gradients generate local electrical fields that attempt to maintain macroscopic charge neutrality and that tend to enhance the diffusion; this is the so-called ambipolar diffusion effect. In this case, in the presence of free electrons, a Lorentz-force term proportional to the locally induced electric field $\mathbf{E}$ will be added to the RHS of Eqs. (11)

and (12). If the electron current is ignored, which is what it is assumed in the adiabatic approach for deriving the Yukawa potential, then $e\mathbf{E} = -\nabla\mu_e$, where μ_e is the electron chemical potential, as well as a heat exchange term proportional to the electron temperature gradient. The chemical potential part adds the term

$$\left(\frac{Z_1^*}{m_1} - \frac{Z_2^*}{m_2}\right)\nabla\mu_e$$

to Eq. (11) (for ionic and neutral components). This introduces terms in Eq. (12) that can be expressed with gradients of electron pressure P_e and electron temperature T_e. The temperature gradient term is again usually combined with the electronic heat exchange (Soret) term. For an ideal, isothermal, nondegenerate binary mixture, we obtain the well-known result [50–52] for barodiffusion:

$$\mathbf{j}^c = -\rho D_{12}\left[\nabla c + c(1-c)\frac{(m_2-m_1)}{\langle m\rangle}\frac{\nabla P_i}{P_i} + c(1-c)\frac{(m_2Z_1^* - m_1Z_2^*)}{\langle m\rangle}\frac{\nabla P_e}{P_e}\right] \quad (13)$$

A noteworthy property of this result is that the diffusion is enhanced over the Fickian component even when there is total pressure balance ($P \equiv P_i + P_e$ = constant); in this case, assuming that the charge states do not vary, one finds

$$\mathbf{j}^c = -\rho D_{12}\Phi_e\nabla c, \quad (14)$$

where,

$$\Phi_e = \frac{\langle Z^*\rangle + \langle (Z^*)^2\rangle}{\langle Z^*\rangle + \langle Z^*\rangle^2}. \quad (15)$$

This expression provides a more general form for the electronic "thermodynamic factor" than Boercker inter alia [10, 16], who assumed that $\langle Z^*\rangle \gg 1$. For a binary mixture the factor Φ_e has a maximum value of

$$\Phi_e|_{max} = 1 + \left(\sqrt{(Z_1^*)(1+Z_2^*)} - \sqrt{(Z_2^*)(1+Z_1^*)}\right)^2, \quad (16)$$

at a given mole fraction that changes with the charge asymmetry of the mixture. This value is unity when $Z_1^* = Z_2^*$. Use of the more general barodiffusion expression automatically (and more accurately) accounts for this enhancement. Modeling and measurement of the thermodiffusivity coefficients that arise in the coupled mass-heat diffusion problem are much more difficult and will be deferred.

III. GREEN-KUBO TECHNIQUE FOR EXTRACTING SELF AND INTERDIFFUSIVITY

The presence of an interface in a system of n-component fluids imposes gradients on different thermodynamic fields in the system. These gradients provide the driving force that mixes the different components into each other smearing out the initial interface and resulting in an eventual uniform mix of the system. If one tracks the interface as it smooths out in time we can extract transport coefficients that enter in the hydrodynamics.

In a more simplistic approach we can address the question of transport coefficient dependence by focusing sequentially in different given situations with a particular composition, temperature and density and allow the system for occasional smooth fluctuations of the composition (or other fields) around the nominal value. By assuming small fluctuations we can exploit the linear response theory in the form of the Green-Kubo (GK) or fluctuation-dissipation approach. These techniques have been frequently used to extract the linear transport coefficients in equilibrium ensembles. The main hypothesis is that the relaxation of a system from spontaneous fluctuations is governed by the same transport coefficients as the relaxation of a fully non-equilibrium system to equilibrium in the limit of linear process.

A. Self-Diffusivity of a tagged particle

One of the most widely known and used GK expressions determines the self-diffusion (or tracer diffusion in mixtures). The self-diffusion coefficient $D_i (i = 1, 2)$ is related to the random-walk motion of a tagged particle of species i in a mixture. It can be calculated from the velocity autocorrelation function $C_i(t)$ via a Green-Kubo integral [45, 47, 53–56],

$$D_i = \int_0^\infty C_i(t)\mathrm{d}t. \quad (17)$$

For an isotropic fluid the velocity auto-correlation function of species i is defined as:

$$C_i(t) = \frac{1}{3}\langle \mathbf{v}^{(i)}(t)\cdot\mathbf{v}^{(i)}(0)\rangle, \quad (18)$$

where in this case the angled brackets denote an ensemble average, here an average of the dot product of an ion's velocity at time t with the same ion's velocity at time 0 for ion type i. The autocorrelation function $C_i(t)$ depends on the species as well as temperature, density and composition. The autocorrelation starts at $C_i(0) = k_BT/m_i$ and decreases toward 0 with time. For moderate to strong coupling mixtures the autocorrelation function exhibits an oscillatory decay, including negative correlations. Negative correlation is a manifestation of the cage effect [57], where the tagged particle finds itself momentary trapped by its immediate neighbors, and the negative correlation results from the velocity reversal as the particle bounces off the cage. At low enough coupling the autocorrelation function decays monotonically, absent the aforementioned many-body effects.

It is straightforward [45, 48] to verify the equivalence of Eq. (18) with the equation relating the mean-squared

displacement of a tagged diffusing particle time, in the long-time limit. This is given by the well known relation due to Einstein for Brownian motion [58]:

$$D_i = \lim_{t\to\infty} \frac{1}{6t}\langle|\mathbf{r}_i(t) - \mathbf{r}_i(0)|^2\rangle. \tag{19}$$

This equivalence constitutes a simple example of the general $fluctuation - dissipation$ relation [59–62]. It also relates the stochastic process of a random walk in which the mean-square displacement of the walker becomes a linear function of time after sufficiently many collisions and displacements have occurred.

B. Interdiffusion; Maxwell-Stefan Equation

Although self-diffusion plays an important role in describing the kinetics during mixing, it is not sufficient to quantify it. The appropriate quantity for Fickian mixing is the interdiffusion current which involves the relative transport of mass current with respect to another. In a binary mixture this current at the center-of-mass frame is given by [45, 47]:

$$\mathbf{j}^c = \rho_1\mathbf{v}_1 - \rho_2\mathbf{v}_2 = c(1-c)\rho(\mathbf{v}_1 - \mathbf{v}_2), \tag{20}$$

with $\mathbf{v}_i$ and ρ_i the center-of-mass velocity and mass density of species i. This is a special case to a more general definition in the multicomponent mixture of the interspecies mass flux in the center-of-mass frame [48, 63]. A more conceptually feasible definition of interdiffusion is often made in terms of a number flux $X_1X_2n(\mathbf{v}_1 - \mathbf{v}_2)$ instead of a mass flux. The interdiffusion process will be described by the Maxwell-Stefan (MS) equation that relates the number density to the gradient in chemical potential μ_i of species i:

$$\frac{X_1X_2(\mathbf{v}_1 - \mathbf{v}_2)}{D_{12}^0} = \frac{X_1}{k_BT}\nabla\mu_1. \tag{21}$$

The right-hand side of the MS Eq. (21) is proportional to a negative driving force for diffusion of species 1, and the left-hand side expresses an average retarding force on particles of species 1 due to interaction with species 2. The coefficient D_{12}^0 - so-called Maxwell-Stefan diffusion coefficient - is related to the Fickian diffusion D_{12} by a thermodynamic factor that accounts for non-ideal mixing contributions to the free energy.

The Green-Kubo formula for the interdiffusion similar to self-diffusion is obtained by combining Fick's phenomenological equation with the mass conservation Eq. (7), and solving these equations in the frequency domain and reciprocal space. Details are given in Ref. [45, 48]. For a binary mixture the result is:

$$D_{12} = \frac{\Phi}{3NX_1X_2}\int_0^\infty dt\,\langle\mathbf{j}(t)\cdot\mathbf{j}(0)\rangle = \Phi D_{12}^0, \tag{22}$$

where $N = N_1 + N_2$ is the total number of particles, and

$$D_{12}^0 = \frac{1}{3NX_1X_2}\int_0^\infty dt\,\langle\mathbf{j}(t)\cdot\mathbf{j}(0)\rangle = \int_0^\infty dt\,C_{MS}(t). \tag{23}$$

In the above we have introduced the MS diffusivity correlation function: $C_{MS}(t) = \langle\mathbf{j}(t)\cdot\mathbf{j}(0)\rangle/(3NX_1X_2)$. Here $\mathbf{j}(t)$ is given by:

$$\mathbf{j}(t) = X_2\sum_{\alpha=1}^{N_1}\mathbf{v}_\alpha - X_1\sum_{\beta=1}^{N_2}\mathbf{v}_\beta = NX_1X_2(\mathbf{v}_1 - \mathbf{v}_2), \tag{24}$$

representing number flux instead of the mass flux $\mathbf{j}^c(t)$ in Eq. (20). The prefactor Φ is the thermodynamic factor whose presence stems from the definition of Fickian diffusion in terms of the gradient in mass fraction rather than gradient in chemical potential which enters in Maxwell-Stefan diffusion. The thermodynamic factor in Eq. (22) is defined by $\Phi \equiv \lim_{k\to0} X_1X_2/S_{XX}(k)$. In the above $S_{XX}(k)$ is the concentration structure factor defined in terms of partial structure factors $S_{ij}(k) = \frac{1}{N}\sum_{\alpha=1}^{N_i}\sum_{\beta=1}^{N_j}\langle\exp i\mathbf{k}\cdot(\mathbf{r}_\alpha - \mathbf{r}_\beta)\rangle$, with i, j the species indices, by the following relation due to Bhatia & Thornton [64]:

$$S_{XX}(k) = X_2^2S_{11}(k) + X_1^2S_{22}(k) - 2X_1X_2S_{12}(k). \tag{25}$$

In the long wavelength limit $k \to 0$ all the structure factors can be derived by either thermodynamic fluctuation theory or by calculation in a grand canonical ensemble [65]. By following either of these approach the concentration structure factor in isobaric-isothermal conditions is given by:

$$S_{XX}(0) = 1/\left(\frac{\partial^2(\beta G/N)}{\partial X_1^2}\right)_{P,T}, \tag{26}$$

and therefore we can express the thermodynamic factor as:

$$\Phi = X_1X_2\left[\frac{\partial^2(\beta G/N)}{\partial X_1^2}\right]_{P,T}. \tag{27}$$

With this new definition (27) it is clear that the thermodynamic factor Φ accounts for non-ideal mixing contributions to the Gibbs free energy. For ideal mixtures this factor is unity which results in Maxwell-Stefan and Fickian diffusivity being identical. For ionic mixtures this factor is larger than one, due to ambipolar effect, depending on the symmetry of the mixture. For a mixed plasma in a rigid background of electrons the difference from the ideal mixture arises from entropic effect induced by this neutralizing background as mixing occurs [10, 16]. As it was shown in the Hydrodynamics Section the thermodynamic factor is: $\left(\langle Z^*\rangle + \langle(Z^*)^2\rangle\right)/\left(\langle Z^*\rangle + \langle Z^*\rangle^2\right)$ which in the limit $\langle Z^*\rangle \gg 1$ goes to $\langle(Z^*)^2\rangle/\langle Z^*\rangle^2$. This factor increases with the asymmetry of the mixture.

For plasma mixtures immersed in a polarizable electron background, deriving this factor requires a full knowledge of the plasma EOS. In this work we focus on computing only the Maxwell-Stefan diffusivity.

IV. METHODS

An extremely powerful, albeit simple, tool to calculate diffusion coefficients is MD simulation. MD simulations follow the motion of atoms (ions) by integrating their equations of motion while accounting for the pairwise particle-particle interactions [66, 67]. The atoms move according to the Newton's Second Law:

$$m\ddot{\mathbf{r}}_i = \sum_{i\neq j}^{N} \mathbf{F}_{i,j}(t). \tag{28}$$

This set of $3N$ coupled ordinary differential equations are integrated explicitly in time using the velocity Verlet [66] algorithm, with a time step that is related to the characteristic time scale of the system. Here N is the total number of particles in the system. In Eq. (28), $\mathbf{F}_{i,j}$ is the force originating from the interaction of particle i with particle j. We study an unconfined system of particles which entails use of the periodic boundary conditions (PBC).

We use this general tool to study our plasma system as a mixture of partially ionized deuterium (D) and argon (Ar). The interaction force $\mathbf{F}_{i,j}$ among these ions has a Coulombic nature. The presence of free electrons, that act as a neutralizing background, results in an effective ion-ion interaction potential. Within linear response theories [34, 35] the interaction between ions is the Yukawa potential:

$$\phi(\mathbf{r}_{ij}) = \frac{Z_i Z_j e^2}{4\pi\epsilon_0 r_{ij}} \exp(-r_{ij}k_{D,e}), \tag{29}$$

where $1/k_{D,e}$ is the screening length due to the electrons.

A. Effective ion-ion potential: Screening

This effective potential between the ions is derived from the electron density distribution in space when the ions are embedded in their midst. Finite temperature Thomas-Fermi techniques start with consideration of the Poisson equation:

$$\frac{\epsilon_0}{e}\nabla^2\phi(\mathbf{r}) = \sum_i Z_i^*\delta(\mathbf{r}-\mathbf{r_i}) - 2\int \frac{d^3p}{(2\pi\hbar)^3} \times \left[1+\exp\left(\frac{p^2/2m_e + e\phi(\mathbf{r}) - \mu_e}{k_BT}\right)\right]^{-1} \tag{30}$$

where μ_e is the chemical potential of the unperturbed electron fluid. In the linear response limit the screening length that enters in the Yukawa potential (29) is:

$$\lambda_{D,e} = \sqrt{\left(\frac{\epsilon_0\Lambda_e^3 k_BT}{e^2 I_{-1/2}(\mu_e/k_BT)}\right)} = \\ = k_{D,e}^{-1} \approx \sqrt{\frac{\epsilon_0\sqrt{(k_BT)^2 + \left(\frac{2}{3}E_F\right)^2}}{n_e e^2}}, \tag{31}$$

where $I_{-1/2}(y) = \int_0^\infty \frac{x^{-1/2}\mathrm{d}x}{1+\exp(x-y)}$, is the Fermi integral of order $-1/2$, $\Lambda_e = \sqrt{2\pi\hbar^2/k_BTm_e}$ is the electron de Broglie wavelength. The last term in Eq. (31) represents a Debye-Hückel [68] form of the screening coefficient with an effective temperature that accounts for the partial degeneracy of the electrons by use of the Fermi energy $E_f = \hbar^2(3\pi^2 n_e)^{2/3}/2m_e$ [43, 69]. Considering the global charge neutrality, the electron density can be related to ion density and the average charge $\langle Z^*\rangle$ of the mixture by $n_e = \langle Z^*\rangle n$. In Fig. 4, we plot the electron screening length computed from Eq. (31) for different temperatures and compositions. Also for comparison ionic and electronic Wigner-Seitz radii are shown in the same plot. In this case, as done for all this work, we vary the mole fraction of the mixture keeping the ion number density constant at 10^{25} ion/cm^3. This is clearly indicated in Fig. 4 where the Wigner-Seitz radius remains the same with composition. Due to global neutrality, the electron density on the other hand increases with the Ar mole fraction, and as a result the screening length decreases.

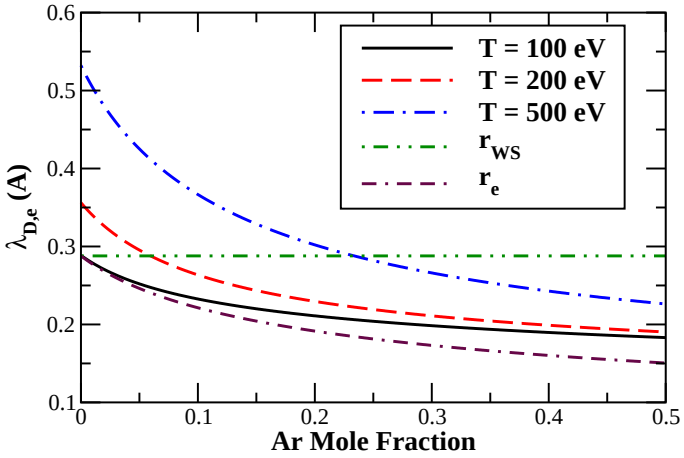

FIG. 4. (Color online) Electron screening length $\lambda_{D,e}$ computed using Eq. (31) as a function of Ar mole fraction in a D-Ar mixture at T = 100, 200 and 500 eV, density 10^{25} ion/cm^3, and ionization $Z^*_{\mathrm{D}} = 1$ and $Z^*_{\mathrm{Ar}} = 13$.

B. Details of the MD simulations

The screening length sets an important length scale for the system. Yukawa systems can be described by the

dimensionless screening coefficient $\kappa = r_{WS}\, k_{D,e}$ [3] and the effective coupling $\Gamma_{\rm eff}$. These are the only two dimensionless parameters of a single-species Yukawa system. When the screening coefficient $\kappa \geq 1$ is large the Yukawa potential is a short range potential. In this case it is computationally advantageous to use a truncation of the interaction potential, limiting the need to sum pairwise ion-ion interactions only to those ions situated within a (κ-dependent) cutoff radius.

The MD simulations [70] presented here are initiated from a spatially random particle configuration, and particle velocities sampled from a Maxwellian distribution of a given temperature T. The random configuration of the particles of each component ensures a spatially uniform mixture as well, suitable for equilibrium MD. The system is initially equilibrated at the desired temperature using a Nosé-Hoover [66, 71, 72] thermostat (constant number of particles N, volume V and temperature T). On average the system is left to equilibrate for 50000 timesteps in this NVT ensemble. The subsequent production run to calculate the diffusivity is done in a microcanonical ensemble with constant N, volume V and total energy E.

To calculate the diffusion coefficients of a binary mixed plasma of D with Ar we have performed MD simulations at temperatures $T = 100$, 200 and 500 eV, particle number density $10^{25}/\mathrm{cm}^3$. We input the ionization as a free parameter independent of the thermodynamic conditions of the mixtures. The physical ionization can be determined by an average atom Thomas-Fermi approximation (Section V B), but we keep it as an adjustable parameter. We chose fully ionized deuterium and ionization of Ar with values $Z^*_{Ar} = 4, 8, 13$ and 18. The screening length that enters the Yukawa ion-ion potential was computed by using relation (31). For each of the above condition we also consider mixtures whose Ar mole fraction is: $X = 0.01$, 0.05, 0.1, 0.2 and 0.5. The calculations were performed with enough particles ($30000 \geq N \geq 120000$) over long enough time scales to ensure convergence with insignificant statistical uncertainty (less than 5%).

The time scale of the system is set by the ionic plasma frequency

$$\omega_p = \sqrt{\frac{e^2 \langle Z^* \rangle^2 n}{\epsilon_0 \langle m \rangle}}. \tag{32}$$

The timestep in the runs was taken as $\Delta t \simeq 1/(\varpi \omega_E)$, where ω_E is the Einstein frequency, that physically describes the oscillatory motion of a caged particle in the well potential created by its neighbors, and the coefficient ϖ had values in the range $100 \leq \varpi \leq 1000$. The values of ϖ were chosen such that the time step is small enough to accurately resolve the trajectory of particles before and after collisions. For most of the cases that we studied the value of $\varpi = 300$ was used. However for a few situations, with $T = 500$ eV, $X \leq 0.1$ and $Z_{Ar} = 13$, we needed to reduce the timestep by a factor of ten ($\varpi = 1000$) to resolve strong binary collisions events. In the limit of no screening $\kappa \to 0$ we have $\omega_E = \omega_p/\sqrt{3}$ [3], and for a finite screening we use a form $\sqrt{3}\,\omega_E(\kappa) = \omega_p \exp(-0.2\kappa^{1.62})$ [69] fitted to the Ohta and Hamaguchi MD results [3].

The autocorrelation functions were computed on the fly as the simulation progressed. For the velocity autocorrelation function (18), the initial velocity $\mathbf{v}(0)$ is saved for each ion. The simulation was run in parallel supercomputers and so the initial velocity together with other ion attributes has to be communicated when an ion moves from a spatial domain related to one processor into another.

The correlation functions are saved as a table for a sufficiently large time span t_{max}. The diffusivity was then computed by postprocessing as:

$$\mathcal{D} = \int_0^\infty dt\, \mathcal{C}(t) \approx \left[\sum_k^{t_{max}/\Delta t} a_k \Delta t \mathcal{C}(t_k) \right] + \Psi(t_{max}), \tag{33}$$

where the coefficients a_k give the Simpson's rule approximation to the integral. The long-time tail contribution was included by the second term in the right-hand side of Eq. (33) with, $\Psi(t_{max}) = \int_{t_{max}}^\infty dt\, \mathcal{C}(t)$. The tail of the correlation function is usually modeled by an analytical form. For the VAF of hard-spheres it was shown [73] that the long-time tail decays as $t^{-3/2}$. Rudd et al. [47], accounted for a more general power law $t^{-\alpha}$ decay in the correlation function. They found that the value of exponent α ranges from 3/2 up to $\alpha \sim 2$. In this case the contribution to diffusion from the tail is:

$$\Psi(t_{max}) = \frac{t_{max}}{\alpha - 1} \mathcal{C}(t_{max}). \tag{34}$$

For the conditions that we consider in our simulations the tail contribution was small (less than 5%).

An approximation of the mean free path $l_{\rm mfp}$ of each species can be calculated from the self-diffusivity assuming the relationship from the kinetic theory of gases:

$$l_{\rm mfp} = \frac{3\mathcal{D}}{v_{th}}. \tag{35}$$

$v_{th} = \sqrt{8 k_B T/\pi m_{red}}$ is the thermal velocity. We use the self-diffusivities from our previous study [48] and Eq. (35) to compute the mean free path of each component. For a D-Ar mixture with 1% Ar mole fraction at $T = 100$ eV, and ion density $10^{25}/cc$, the mean free path $l_{\rm mfp}$ is 1.159 and 4.551 Å for Ar and D, respectively. The mean free path decreases as the Ar mole fraction increases, with the temperature and total number density fixed, so these are the largest values of the mean free path in the $Z^*_{\rm Ar} = 13$ systems. The 30000-ion simulation at $n = 10^{25}\,\mathrm{ion/cm}^3$ has box edges of 14.4 Å, which is 3.15 times larger than the mean free path of the lighter species D. Also the mean free path of Ar and D are 1.34 and 15.8 times larger than the r_{WS} at this density. So the simulation box is

sufficiently large compared to the mean free path to avoid Knudsen-like finite size effects. The Ar mean free path is comparable to the inter-ionic spacing, especially at larger Ar mole fractions, and the effects of this can be seen as structure in the Ar velocity autocorrelation functions for $X \geq 0.2$ [48].

V. RESULTS AND DISCUSSIONS

We present results from MD of diffusivity in a binary mixture for different conditions. The effect of composition on transport can initially be studied by computing the self-diffusion coefficient of each component in the binary mixture for different compositions, temperatures and densities. The self-diffusivity is related to the motion of tagged particle, which can be conveniently computed by making use of the Green-Kubo approach, by computing the velocity autocorrelation function (VAF) of a tagged particle. Self-diffusivity in D-Ar mixtures has been investigated with MD previously [48], showing a general trend of the self-diffusivities to increase with temperature and to decrease with the increasing density, Ar ionization and Ar mole fraction. It was also observed that at compositions with trace element Ar the self-diffusivity of D is almost unaffected from the ionization of Ar.

A. Maxwell-Stefan diffusivity

To compute the Maxwell-Stefan (MS) diffusivity coefficient using the Green-Kubo technique we need to evaluate the interdiffusion current correlation function

$$C_{\rm MS}(t) = \frac{1}{3}\langle \mathbf{j}(t)\cdot\mathbf{j}(0)\rangle \qquad (36)$$
$$= \frac{X_1X_2N}{3}\langle[\mathbf{v}_1(t)-\mathbf{v}_2(t)]\cdot[\mathbf{v}_1(0)-\mathbf{v}_2(0)]\rangle,$$

where the interdiffusion current $\mathbf{j}(t)$ is given by Eq. (24). In Fig. 5 we present plots of the $C_{\rm MS}$ for different compositions at 100 eV. The ionizations of deuterium and argon were kept constant at 1 and 13, respectively, while the composition of the binary mixture varied from 1% to 50% argon mole fraction. The ion number density was 10^{25} ion/cm^3. In Fig. 5 correlation functions are plotted versus time for Ar mole fraction $X = 0.01$, 0.05 and 0.1. In general the correlation functions are expected to decay exponentially initially and switch to slower power law decay at long times due to memory effects and hydrodynamic modes [45]. Since the temperature is very high, large fluctuations in the tail of the $C_{\rm MS}$ correlation function obscure the form of its long-time decay. As seen in Fig. 5, the exponential decay of the correlation function extends to 10 fs or more, and the contribution from the long-time tail is insignificant. We can therefore fit the correlation functions with exponential expressions $\sim A_0\exp(-t/\tau_c)$, where A_0 is a coefficient, and τ_c is a characteristic correlation time. This form indicates that the sequence of the collective collisions between different ions form a Poisson process [45, 62]. For the dense plasma that we are considering here this is not necessary true if we reduce T and increase the coupling in which case we would need to fit the power-law tail or invoke mode coupling theory to predict its form. With increasing argon mole fraction in the mixture, the electron density increases so that the coupling and the screening coefficient entering the effective ion-ion Yukawa also increase. As expected the exponential decay constant τ_c decreases as we increase the mole fraction of Ar due to stronger scattering. The faster decay of the $C_{\rm MS}$ for the highest Ar mole fraction demonstrates this decrease. The correlation functions have been time averaged over 2×10^7 time steps to improve the statistics and reduce the fluctuations at the tails.

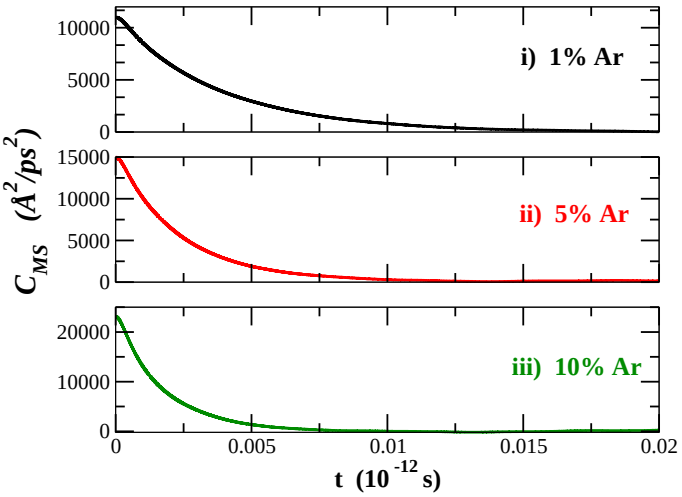

FIG. 5. (Color online) The interdiffusion current correlation function $C_{\rm MS}$ as a function of time that enters in the MS diffusion plotted for different compositions of binary ionic mixture at 100 eV and 10^{25} ion/cm^3.

Integrating $C_{\rm MS}$ in time we can extract diffusion as a function of time t_{max}, where t_{max} is the cutoff value in the numerical integral.

In Fig. 6 we plot these partial integrals of the $C_{\rm MS}$ for the same cases as in Fig. 5. These can be fit with functions of the form

$$D_{\rm fit}(t) = A\left[1-\exp\left(-\frac{t}{\tau_c}\right)\right], \qquad (37)$$

where A is a coefficient that gives the correct diffusion value ($D^0_{12} = A$).

In Fig. 7, we plot the computed values of the MS diffusivities as a function of composition for three different T. As mentioned before, we kept the volume of the system constant as the composition is changed. With this choice it can be seen that the diffusion is not a strong function of composition. At 100 eV the results are particularly flat, with the MS diffusivity at ~ 0.004 cm^2/s

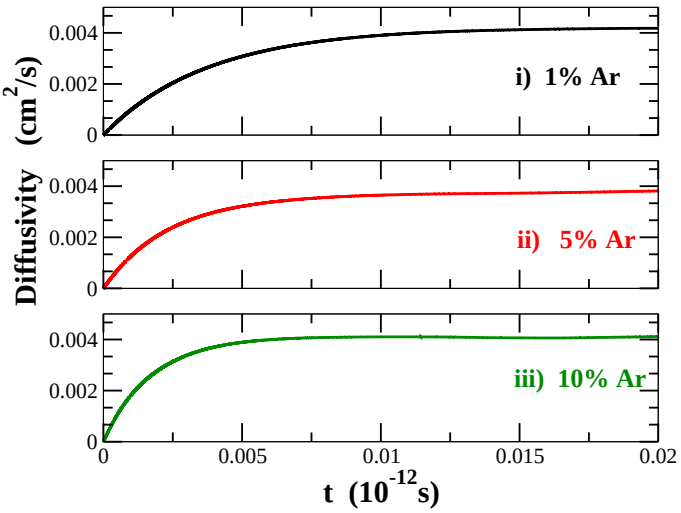

FIG. 6. (Color online) Time dependent Maxwell-Stefan diffusivities from the partial integrals in time of the correlation functions shown in Fig. 5.

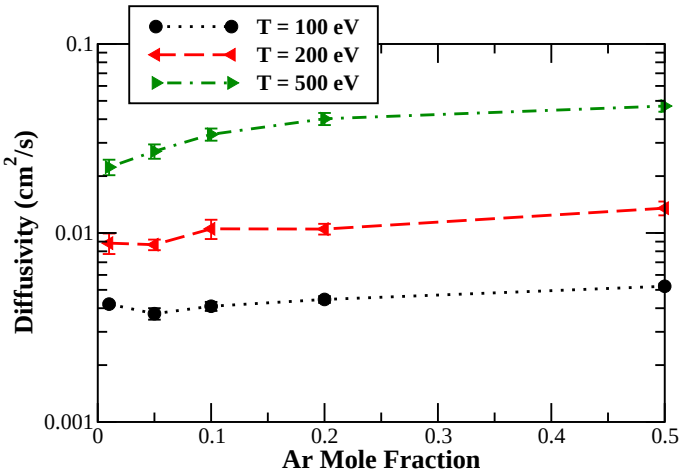

FIG. 7. (Color online) Maxwell-Stefan diffusion for different temperatures and Ar composition in the mixtures. Ionization of both D and Ar was entered as a free parameter and kept constant at values 1 and 13, respectively.

for all of the compositions studied. At higher T the value of MS diffusivity asymptotes to a constant beyond some composition threshold value that increases with T. For $T = 500$ eV the value of MS diffusivity is changing from ~ 0.02 cm^2/s at $X = 0.01$ to ~ 0.045 cm^2/s at $X \geq 0.2$. We ran the same simulations over different replicas, and an error estimate for the diffusivity was derived from the scatter, with the result shown as the error bars in the figure.

B. Diffusivity as a function of mean ionization state

In the previous Section we computed the MS diffusivity at a given ion density by changing the temperature and composition while keeping the ionization fixed. The ionization was chosen near a physical value while also providing a case study of an asymmetric mixture. Here we assess the role of the ionization on MS diffusivity. Although we choose the ionization as a free parameter it is also very helpful to compare the physical value for the ionization.

The mean ionization value in the warm and hot dense plasma regimes may be computed through the use of average atom Thomas-Fermi approach [30, 43, 74–77]. For the one-component ionic plasma the properties, including ionization, are approximated with those of single neutral spherically symmetric atom of radius r_{WS}. The ionization will be defined as

$$Z^* = Z - \int d^3r\, n_b^e(r), \tag{38}$$

where Z is the nuclear charge, and $n_b^e(r)$ is the density of the bound electrons whose kinetic energy is smaller than the potential such that $p^2/2m_e - eV(r) < 0$. The electrons satisfy the Fermi-Dirac statistics so their density in space is given by

$$n_b^e(r) = \frac{8\pi}{h^3} \int_0^{\sqrt{-2m_e V(r)}} \frac{\mathrm{d}p\, p^2}{1 + \exp\left(\frac{p^2/2m_e - eV(r) - \mu_e}{k_B T}\right)} \tag{39}$$

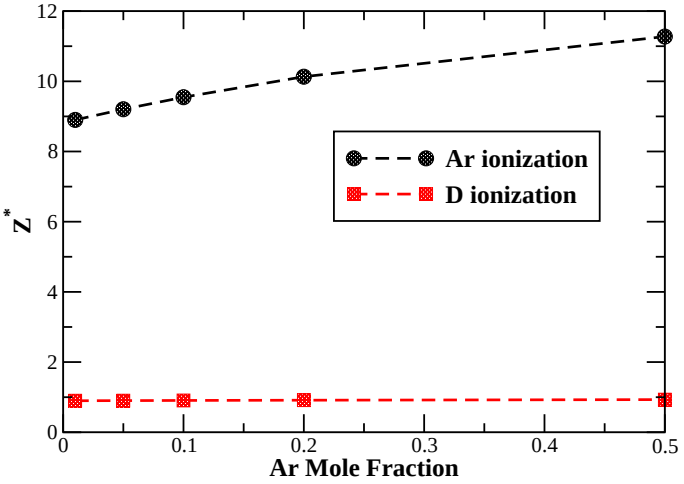

FIG. 8. (Color online) Values of Ar and D ionization as a function of composition of a D-Ar mixture at $T = 100$ eV and ion number density 10^{25}ion/cm^3. The values were computed using an average atom Thomas-Fermi approach.

In a binary mixture holding the total number density of ions fixed, the mean ionization state of each species depends on the composition. We have chosen to compute

the ionization by combining single-species results from Eqs. (38) and (39) using the so-called volume additivity mixing rule [32, 78] or Agamat's Law. At a given temperature and pressure, the number densities and ionizations of the two pure components are calculated. To get the mixture equation of state, the reciprocals of the number densities are added, weighted by the mole fractions, to get the total volume and, hence, the total density. The ionizations of the species in the plasma mixture are taken to be the same as the ionizations in the pure plasmas. Results of this analysis are shown in Fig. 8, where we plot values of the mean ionization state for the Ar and D in a binary mixture at the temperature 100 eV and the density 10^{25} cm^{-3} as a function of Ar mole fraction. The ionization of D is very close to 1, justifying our choice of fully ionized D. However, the ionization of Ar is increasing almost linearly with composition from a value of 8.9 at 1% to 11.3 at 50% Ar. It should be noted that these values of ionization are approximate and depend on the definition of the bound electrons [43] and the mixing scheme.

We turn now to computing the coefficient of diffusivity with MD for a given set of conditions while varying the ionization as a free parameter. In Fig. 9 we plot results from such analysis. The results correspond to a particular composition with 10% Ar at 100 eV and number density 10^{25} ion/cm^3. We set the ionization of D at 1, which is a reasonable approximation as suggested from our average atom Thomas-Fermi analysis, and varied the ionization of Ar as a free parameter. Results for the D and Ar self-diffusivities are plotted along with MS diffusivity in Fig. 9 and also shown in Table I. The MS diffusivity follows a power law decay $\sim 1/Z^*_{Ar}$ with the ionization. From relation (1) we would have expected a $\sim (Z^*)^{-2}$ decay with the assumption of constant $\ln\Lambda$. We show in the last part of this Article that this is not the case. Similar qualitative behavior is observed from the self-diffusivities.

This plot provides an helpful tool for mapping the values of the ionizations with the expected value of diffusivity. For example, from our Thomas-Fermi and linear-mixing approach we expect that the ionization of Ar at this thermodynamic conditions to be $Z^*_{Ar} \approx 10$, which for MS diffusivity interpolates from Fig. 9 a value $D^0_{12} \approx 0.005$ cm$^2/s$.

C. Empirical models that relate Maxwell-Stefan diffusivity with self-diffusivities

The relation between interdiffusion and self-diffusion of the different species has been widely discussed in the literature. The Green-Kubo form of interdiffusion can be described in terms linear in the self-diffusion coefficients and complicated velocity cross-correlation terms. If we group separately the velocity autocorrelation and cross-correlation functions that appear in Maxwell-Stefan

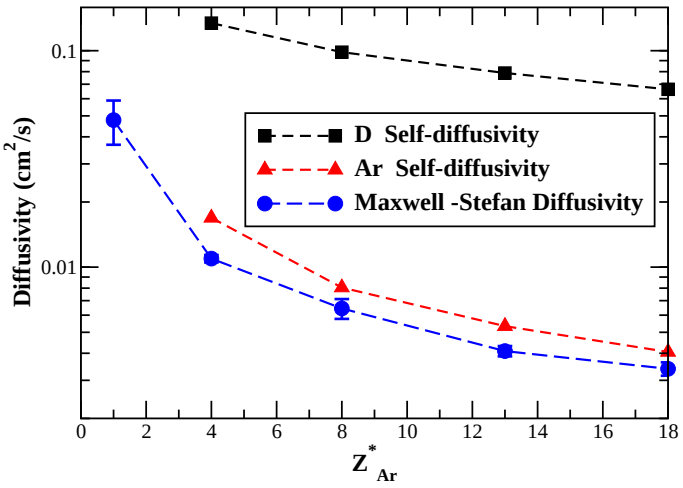

FIG. 9. (Color online) Values of self-diffusivities and mutual diffusivity as a function of the ionization level of Ar. The case presented here corresponds to a 10% Ar binary mixture with deuterium, kept at $T = 100$ eV and number density 10^{25} ions/cm^3. The ionization of deuterium was fixed at 1, while that of Ar was varied.

TABLE I. Self-diffusivity and MS diffusivity values computed from molecular dynamics for binary mixtures of 10% Ar with D, at temperature 100 eV and number density 10^{25}/cm^3. Results are shown for different Ar ionization states $Z^*_{\rm Ar}$.

$Z^*_{\rm Ar}$	$D_{\rm Ar}$ (cm^2/s)	D_D (cm^2/s)	D^0_{12} (cm^2/s)
1			0.04781
4	0.13416	0.01690	0.01095
8	0.09847	0.00805	0.00644
13	0.07889	0.00534	0.00409
18	0.06633	0.00406	0.00339

diffusion coefficient (23) we have the following [63]:

$$D^0_{12} = \left[X_2 D_1 + X_1 D_2 + X_1 X_2 \left(\frac{\mathcal{F}_{11}}{X_1^2} + \frac{\mathcal{F}_{22}}{X_2^2} - 2\frac{\mathcal{F}_{12}}{X_1 X_2}\right)\right], \tag{40}$$

where the $\mathcal{F}$-factors are given by

$$\mathcal{F}_{\alpha\beta} = \frac{1}{3N}\sum_{i=1}^{N_\alpha}\sum_{j\neq i}^{N_\beta}\int_0^\infty \langle \mathbf{v}_i^\alpha(t)\cdot\mathbf{v}_j^\beta\rangle dt. \tag{41}$$

If we assume that velocity cross-correlations are negligible, i.e.,

$$\frac{\mathcal{F}_{11}}{X_1^2} + \frac{\mathcal{F}_{22}}{X_2^2} - 2\frac{\mathcal{F}_{12}}{X_1 X_2} = 0, \tag{42}$$

a simple linear rule results, connecting the Maxwell-Stefan diffusivity with self-diffusity in a binary system

$$D^0_{12} = X_2 D_1 + X_1 D_2. \tag{43}$$

This relation (43) is known in the condensed matter community as Darken's equation [47, 63, 79, 80]. This relation has also been used in the plasma community mainly for binary ionic mixtures [4, 9, 10, 33]. It has been tested to some extent, but to our knowledge no one has done a thorough numerical study to test its accuracy. For many neutral and symmetric mixtures it works reasonably well [63, 81]. As an example, Rudd et al. [47] showed that the computed MS diffusivities and the corresponding diffusivities derived from the Darken relation (43) differ by less than 15% for Al and Cu molten mixtures of any composition across a broad range of pressures and temperatures. The situation is quite different when considering ionic liquids. Computer simulations [45] have shown that there is an appreciable positive correlation between the velocities of neighboring ions which has the effect of inhibiting interdiffusion. In cases where the Darken relation holds or interdiffusivity can be related to the self-diffusivities in a similarly explicit manner, it can be computationally expedient. The Green-Kubo calculation of the self-diffusivity converges more quickly than that of the interdiffusivity. It is thus important to assess if this relation provides a good approximation for the asymmetric plasma mixtures that we are considering. Extending

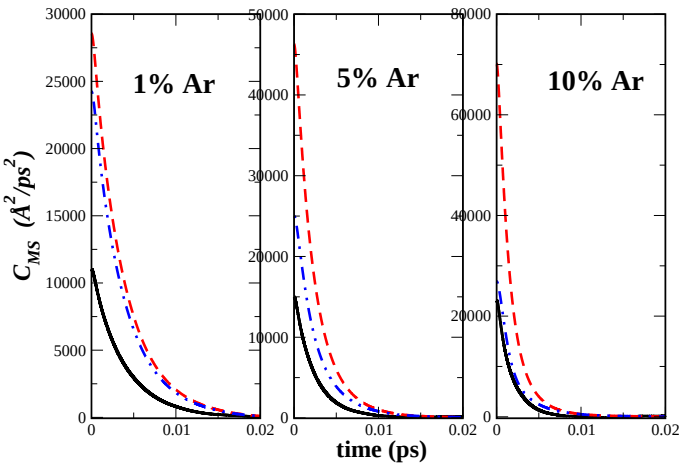

FIG. 10. (Color online) Velocity cross-correlation function for $1, 5$ and 10% Ar. The black solid line is related to the MD calculated Maxwell Stefan diffusivity, the red dashed line is the Darken relation and the blue dot-dashed lined is the common force model.

the Darken relation to the level of correlation functions would give the relation

$$C_{\rm MS}(t) = X_2 C_1(t) + X_1 C_2(t). \qquad (44)$$

If true, it provides a sufficient condition for the verity of the Darken relation (43). So as a first step in Fig. 10 we plot the velocity correlation function as computed from a Darken-like linear combination of velocity autocorrelation function VAF together with $C_{\rm MS}$. As seen from this graph the cross-correlation terms play an important role and that the interdiffusion current correlation function has over all time a smaller value than the Darken-like linear combination of VAF. In Fig. 11 we plot the Maxwell-Stefan diffusivity along with the Darken diffusivity. The latter is a factor of 2 larger than the MS diffusivity for all mole fraction which is a clear indication that correlation between the velocities of neighboring Yukawa ions is significantly reducing interdiffusion. This result contradicts earlier work that found the Darken relation to provide a good description of binary ionic mixtures [4, 9, 10, 33]. A second empirical relation between MS diffusivity and

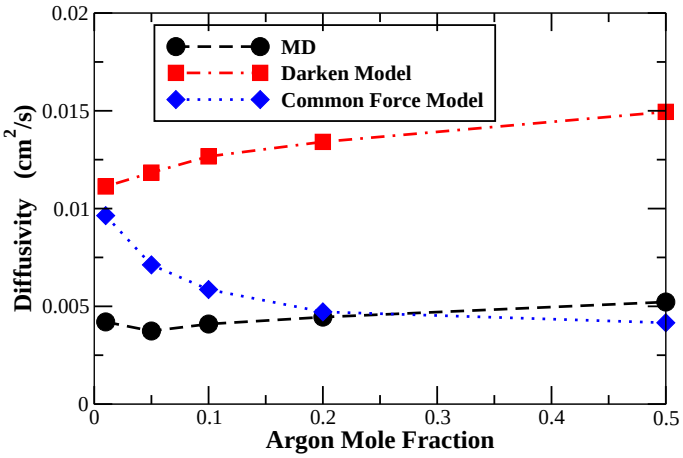

FIG. 11. (Color online) Maxwell-Stefan diffusivities from MD in black, compared with the Darken combination of self-diffusivities in red and Common Force model in blue for different composition of D-Ar mixture at 100 eV and 10^{25} ion/cm^3. The ionizations of D and Ar were 1 and 13, respectively.

self-diffusivity that accounts to some extent for the cross-correlations among neighboring ions can be derived by the use of the *common force model* (CFM) [63]. In this approach, although the thermodynamic forces on a given ion arising from the motion of its neighbors is complicated due to the cross-correlation terms, we can simplify the problem by following a mean-field prescription and replace the field of these forces with their average value. For each species the individual number flux will be a product of the species mobility D_i/k_BT and a thermodynamic driving force. The driving force has two contributions; from a diffusive term which is proportional to $-\nabla\mu_i$, and an advection term that accounts for the cross-correlation terms at a mean-field level and which we can set it constant to a common value F. Following the above prescription each individual number flux can be described as

$$\mathbf{j}_i = nX_i \frac{D_i}{k_BT}\left(-\nabla\mu_i + F\right), \qquad (45)$$

with n the ion number density. Like other empirical diffusivity relations, the common force model effectively introduces a background current that is set by imposing a frame of reference. Here imposing no net flux, $\mathbf{j}_1 + \mathbf{j}_2 = 0$,

the common force F should satisfy

$$F = \frac{X_1 D_1 \nabla\mu_1 + X_2 D_2 \nabla\mu_2}{X_1 D_1 + X_2 D_2}. \quad (46)$$

By use of this form of the F and the Gibbs-Duhem relation $X_1\nabla\mu_1 + X_2\nabla\mu_2 = 0$, the diffusion flux is given by

$$\mathbf{j} = nX_1 \left(\frac{D_1 D_2}{X_1 D_1 + X_2 D_2}\right) \frac{\nabla\mu_1}{k_B T}. \quad (47)$$

Comparing Eq. (47) with the Maxwell-Stefan relation Eq. (21) we come to the following CFM relation between MS diffusivity and the self-diffusivities

$$D_{12}^0 = \frac{D_1 D_2}{X_1 D_1 + X_2 D_2}. \quad (48)$$

If we compare Eq. (48) with Eq. (40) then in this approach the cross-correlation terms should satisfy the following relation

$$\frac{\mathcal{F}_{11}}{X_1^2} + \frac{\mathcal{F}_{22}}{X_2^2} - 2\frac{\mathcal{F}_{12}}{X_1 X_2} = -\frac{(D_1 - D_2)^2}{X_1 D_1 + X_2 D_2} \leq 0. \quad (49)$$

In Figs. 10 and 11, we have added the CFM combination (48) of self-diffusivities to compare with the computed MS. As expected CFM provides a better approximation than Darken to MS diffusivity. For Ar mole fraction in the range $X \geq 0.1$, CFM model is satisfied with an uncertainty of less than 20%. At very low Ar mole fraction there still is a considerable discrepancy between CFM and MS. One might expect this discrepancy to decrease as the asymmetry of the mixture is reduced, but this is not the case when the density and temperature are held fixed. In Fig. 12 we plot MS along with Darken and CFM diffusivities for a mixture with 10% Ar mole fraction as a function of the Ar ionization Z^*_{Ar}. Interestingly, as we decrease Z^*_{Ar} the discrepancy between the computed MS diffusivity and the empirical models is increasing. The ionic asymmetry of the mixture decreases with Z^*_{Ar}, but the mass asymmetry remains the same, contributing to an increase in cross-correlation of velocities.

A similarity exists between Eq. (44) and the Nernst-Einstein relation, which is an empirical relation that links the electrical conductivity of an ionic system to the self-diffusion coefficients of the cations and anions in the system [82]. In this case the electrical conductivity is related to the same velocity correlation functions as the one that expresses the interdiffusion coefficient.

D. Comparison with kinetic theories

In this Section we compare the MD results with kinetic theory computations of diffusion. As mentioned in the introduction the kinetic equations are based on many simplifying assumptions, like molecular chaos, and binary collisions, while ignoring correlation effects. From

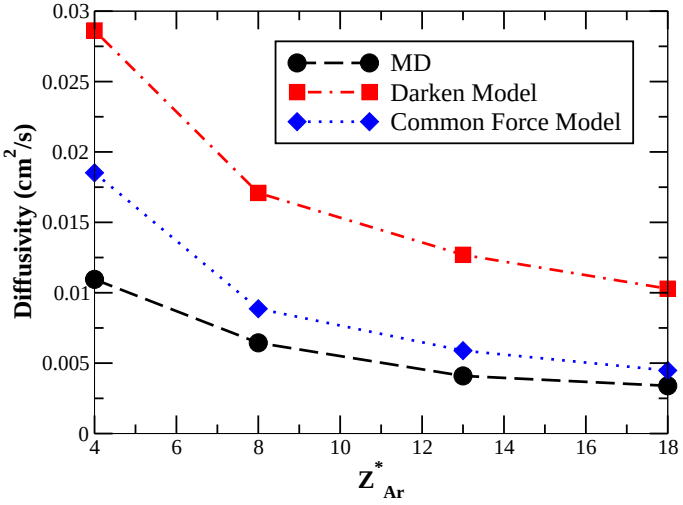

FIG. 12. (Color online) Maxwell-Stefan diffusivities from MD in black, compared with the Darken combination of self-diffusivities in red and Common Force model in blue for a D-Ar mixture with 10% Ar, as a function of Ar ionization Z^*_{Ar}. The mixture was kept at 100 eV and number density 10^{25} ion/cm^3. The ionizations of D was kept at 1.

a microscopic perspective, the hydrodynamic equations can be derived from the Boltzmann equation [1, 49, 83]

$$\left[\frac{\partial}{\partial t} + \mathbf{v}_i \cdot \nabla_{\mathbf{r}} + \mathbf{a} \cdot \nabla_{\mathbf{v}}\right] f_i = \sum_j \hat{\mathcal{C}}_B(f_i, f_j) \equiv \frac{df_i}{dt}|_{coll}, \quad (50)$$

$f_i(\mathbf{r}, \mathbf{v}, t)$ is the one particle distribution function in phase space of species i; $\hat{\mathcal{C}}_B(f_i, f_j) = \int d^3v_j \int d\phi\, d\theta\, \sin\theta\sigma_{ij}\, |\mathbf{v}_i - \mathbf{v}_j| \left(f_i(v_i) f_j(v_j) - f_i(v_i') f_j(v_j')\right)$ is the Boltzmann collision operator in the molecular chaos assumption, with σ_{ij} denoting the scattering cross section. In the macroscopic limit the hydrodynamic equations (7), (8), (9) are derived from velocity moments [83] of the aforementioned kinetic equation (50).

In the Chapman-Enskog [1] approach of solving the Boltzmann Kinetic equation, transport coefficients are given through the collision integrals $\Omega_{ij}^{(lk)}$ between particles of species i and j which are related to the total cross section after integrating over a Maxwellian velocity distribution. They are given by [1, 14]

$$\Omega_{(ij)}^{lk} = \sqrt{\left(\frac{k_B T}{2\pi m_{red}}\right)} \int_0^\infty e^{-g^2} g^{2k+3} \sigma_{ij}^{(l)}\, dg, \quad (51)$$

where $g \equiv |\mathbf{v}_i - \mathbf{v}_j|/v_{ij}$, is a dimensionless velocity with $v_{ij} = \sqrt{2k_B T/m_{red}}$. The reduced mass is $m_{red} \equiv m_i m_j/(m_i + m_j)$ and $\sigma_{ij}^{(l)}$ is the l^{th} momentum transfer cross section for a given energy

$$\sigma_{ij}^{(l)} = 2\pi \int_0^\infty (1 - \cos^l \chi_{ij}) b\, db, \quad (52)$$

with the integration over the impact parameter b.

In Eq. (52) χ_{ij} is the scattering angle given by

$$\chi_{ij} = \pi - 2\int_{r_{ij}^{min}}^{\infty} \frac{b\,dr}{r^2\left[1-\frac{b^2}{r^2}-\frac{V_{ij}(r)}{g^2 k_B T}\right]^{1/2}}. \qquad (53)$$

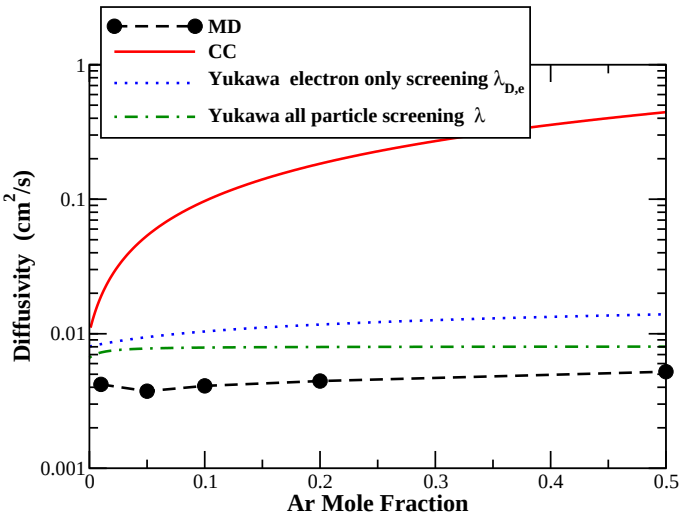

FIG. 13. (Color online) Comparison of MS Diffusion values from MD at 100 eV, 10^{25} ion/cm^3 for D-Ar mixture with kinetic theories based on binary collision approach. The ionizations of D and Ar are 1 and 13, respectively. MD results are represented by symbols connected with black dashed line. Results from Chapman-Cowling (CC) kinetic model assuming a pure Coulombic interaction are in solid red curve. The dotted blue curve and the green dashed-dot curve correspond to results from assuming screened Coulomb with electron screening only (as in MD) and all-particle screening, respectively. For the screened Coulomb cases we used the collision integrals tabulated in Ref. [14].

Here $V_{ij}(r)$ is the interaction potential between the particle of type i and j, and r_{ij}^{min} is the distance of the closest approach between the particles.

In the *first* Chapman-Enskog approximation to transport properties [1], the interdiffusion coefficient is given by

$$\left[D_{12}^0\right]_1 = \frac{3k_BT}{16n\,m_{red}\Omega_{12}^{(11)}}, \qquad (54)$$

where T and n are temperature and ion density. The collision integral can be written as

$$\Omega_{12}^{(11)} = \sqrt{\frac{\pi}{m_{red}}}\frac{\left(Z_1^*Z_2^*e^2\right)^2}{\left(2k_BT\right)^{3/2}}\ln\bar{\Lambda}, \qquad (55)$$

where,

$$\ln\bar{\Lambda} = \frac{\left(2k_BT\right)^2}{2\pi\left(Z_1^*Z_2^*e^2\right)^2}\int_0^{\infty} e^{-g^2}g^5\sigma_{12}^{(1)}\,dg, \qquad (56)$$

is a generalized Coulomb logarithm [6]. From Eq. (54) we then have

$$\left[D_{12}^0\right]_1 = \frac{3}{32n}\frac{\left(2k_BT\right)^{5/2}}{\sqrt{\pi m_{red}}}\frac{1}{\left(Z_1^*Z_2^*e^2\right)^2\ln\bar{\Lambda}} = \frac{\pi}{4}\frac{v_{th}r_{WS}}{\Gamma_{12}^2\ln\bar{\Lambda}}. \qquad (57)$$

Comparing Eq. (57) with Eq. (1) shows $\ln\bar{\Lambda} \to \ln\Lambda$ in the weak coupling limit. In the Chapman and Cowling (CC) [1] approach using the Coulomb interaction potential $V_{ij}(r) = Z_iZ_je^2/r$ and assuming the all-particle Debye screening length as the maximum value for the impact parameter $b_{max} = \sqrt{(\epsilon_0 k_BT)/(n\langle Z^2\rangle + n_e)\,e^2}$, the collision integrals can be computed analytically

$$\ln\bar{\Lambda} = \frac{\ln\left(1+\gamma_{12}^2\right)}{2}, \qquad (58)$$

where $\gamma_{12} = \left(4k_BT\lambda_D\right)/\left(Z_1^*Z_2^*e^2\right)$. In the low-coupling limit $\gamma_{12} \gg 1$, the $\ln\bar{\Lambda} \approx \ln(\gamma_{12}) = \ln\Lambda$.

In Fig. 13 we compare the diffusivity from Chapman and Cowling with the MS diffusivity computed from MD. The CC diffusivity overestimates the MS diffusivity by more than an order of magnitude for much of the range of compositions, which is to be expected since this theory should work at the dilute and low-coupling limit, and it only accounts for the screening in the cutoff value of the Coulomb interaction. A better model with which to compare our MD results is to assume that the ions interact through the Screened Coulomb (SC) interaction $V_{ij}(r) = Z_iZ_je^2\exp(-r/\lambda_{D,e})/r$, with $\lambda_{D,e}$ the screening length due to electrons given by Eq. (31). In this case collision integrals have been computed numerically by Paquette et al. [14]. Other models of the screening are also of interest, as discussed below. We plot the results in Fig. 13. Although results from this model (plotted with dotted blue curve) are on average a factor of 3 larger than MD, they provide a marked improvement over the CC diffusivity.

Both kinetic models ignore correlation effects. From the Darken diffusivity plotted in Figs. 11 and 12 that neglects cross-correlations, we see that much of the discrepancy between the MS diffusivity from MD and the diffusivity from the SC kinetics is already present in the comparison of the MS diffusivity and the Darken diffusivity. This points to cross-correlation being a major contributor to the discrepancy.

The Darken diffusivity does contain some kinds of correlation, such as that due to the average neighborhood of the scattering event which modifies the effective binary collision operator [6, 14, 84]. This correlation is taken into account by Paquette et al. [14] empirically by assuming an effective SC interaction among the ions [14]. The effective screening length λ that enters in the SC potential is not allowed to drop below r_{WS}, which we implement by interpolating between a Debye length λ_D in the dilute limit and r_{WS} in dense case [85]:

$$\lambda = \sqrt{(\lambda_D^2 + r_{WS}^2)}. \qquad (59)$$

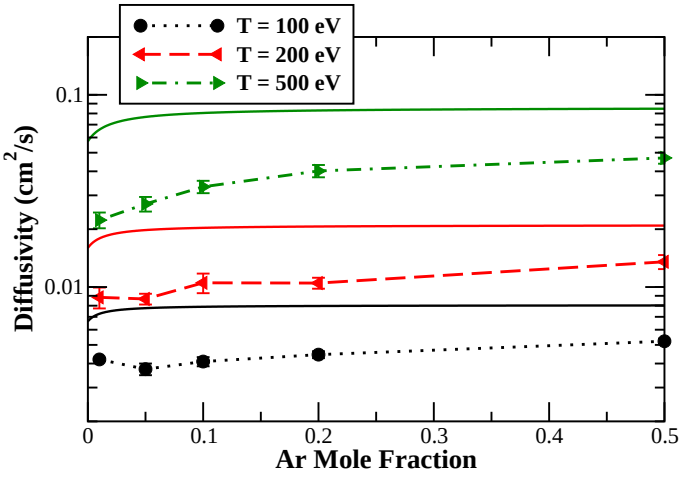

FIG. 14. (Color online) Comparison of MS Diffusion values from MD at 100, 200 and 500 eV, 10^{25} ion/cm^3 for D-Ar mixtures with kinetic theories based on the binary collision approximation. The ionizations of D and Ar are taken to be 1 and 13, respectively. MD results are represented by symbols connected with lines as shown in the legend. Results from kinetic theories based on a screened Coulomb effective ionic interaction are shown with solid curves. For the screened Coulomb cases we used the collision integrals tabulated in Ref. [14]. The effective screening length λ is calculated from Eq. (59).

If there is no screening from the electrons, λ_D will be the Debye screening due to ions only $\lambda_{D,i} = \sqrt{(n\langle Z^2\rangle e^2)/(\epsilon_0 k_B T)}$. For the Yukawa particles (ions dressed by the electron cloud) used in the MD, the appropriate screening coefficient will be one that includes the electron screening as well as all ions. In this case the λ_D that enters in Eq. (59) is

$$\lambda_D = \frac{1}{\sqrt{\lambda_{D,i}^{-2} + \lambda_{D,e}^{-2}}}, \tag{60}$$

with $\lambda_{D,e}$ the screening from partially degenerate electrons from Eq. (31). Results from this analysis are plotted (with dashed-dot green line) in Fig. 13. It gives the best agreement with the MS diffusivity from MD.

In Fig. 14 the diffusivity from SC kinetics (solid lines) is plotted along with the MS diffusivity from MD (symbols) for the three temperatures 100, 200 and 500 eV. Interestingly, there is better agreement between MD and the kinetics models as the Ar mole fraction is increased. Again, the same trend is seen between MS diffusivity and Darken diffusivity from MD, pointing to the importance of cross-correlation. As the screening increases, as with increasing Ar mole fraction, the cross-correlated motion decreases, and as demonstrated previously by Salin and Gilles [11] a better agreement between MD and a good kinetic description is achieved for transport coefficients. In a recent parametric study of one component Yukawa systems [86], it was shown that there is a critical value of screening beyond which transport coefficient computed from MD compares well with kinetics models, and this critical value increases as the coupling of plasma is increased. Referring to Fig. 4 we see that the screening coefficient at a very low Ar concentration decreases by less than a factor of two as we increase T from 100 to 500 eV. The value of the effective coupling Γ_{eff} decreases also proportionally with T. Therefore changes in the screening have an important effect on the diffusivity, even at $T = 500$ eV and low Ar mole fraction.

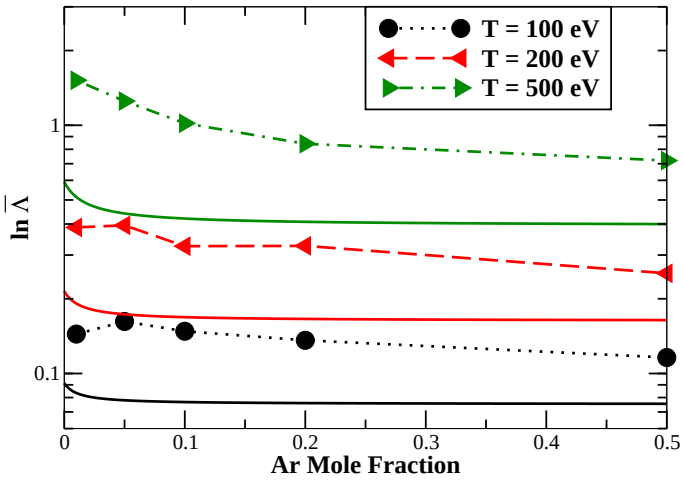

FIG. 15. (Color online) Generalized Coulomb logarithm $\ln\bar{\Lambda}$ from MD as a function of Ar mole fraction for three temperatures $T = 100, 200$ and 500 eV. For comparison we also show the value $\ln\bar{\Lambda}$ from the kinetic theories that use SC potential models with solid lines. The values of $\ln\bar{\Lambda}$ from the kinetics are lower than the ones derived from MD

We have also extracted the generalized Coulomb logarithm $\ln\bar{\Lambda}$ from MD and SC kinetics using the form in Eq. (57). The results are plotted in Fig. 15. The values of $\ln\bar{\Lambda}$ are smaller than 2, which indicates a regime where classic kinetic theories will not work well. In Fig. 16, we plot $\ln\bar{\Lambda}$ for different ionizations of Ar at a mixture with 10% Ar mole fraction at 100 eV. In the same plot results from MD are shown along with the $\ln\bar{\Lambda}$ values from SC kinetics. As we decrease the value of the Ar ionization the effective coupling of the mixture will decrease as well as the screening coefficient. Due to cross-correlation effects that were observed in Fig. 12 the discrepancy between the values of $\ln\bar{\Lambda}$ from MD and SC kinetics increases when Z^*_{Ar} decreases.

Daligault has recently published a model [5] for diffusivity and generalized Coulomb logarithm $\ln\bar{\Lambda}$ based on a MD study of one component Yukawa plasma. His $\ln\bar{\Lambda}$ is a function of the dimensionless screening κ:

$$\ln\bar{\Lambda}(\kappa,\Gamma) = \ln\left(1 + \frac{C(\kappa)}{\sqrt{3}\Gamma^{3/2}}\right), \tag{61}$$

with $C(\kappa)$ a function tabulated in Ref. [5], and Γ the coupling of the single species plasma. To extend this

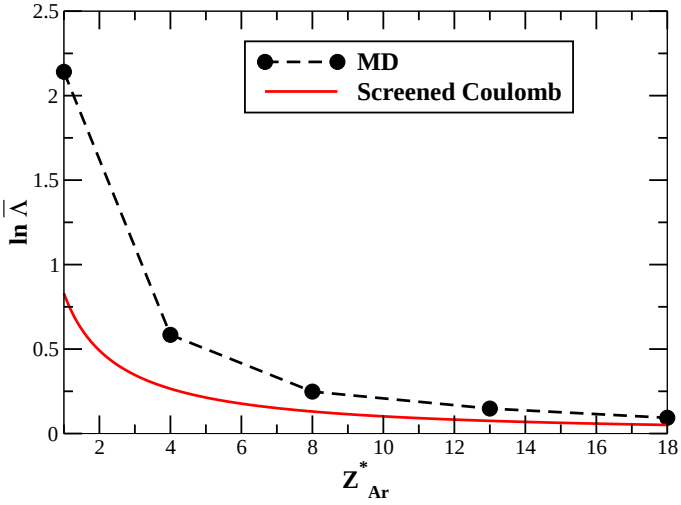

FIG. 16. (Color online) Generalized Coulomb logarithm $\ln\bar{\Lambda}$ as a function of ionization for a 10% Ar mixture at 100 eV. Values extracted from MD (symbols connected with dashed line) are compared with the ones derived from kinetic theory that use SC potential models (red solid line).

model to a plasma with two ionic species is ambiguous since we need a unique relation of Γ to Γ_{eff} or Γ_{12} for the mixture. However, for a mixture of ions with the same charge this form can be used. For a 10% Ar mole fraction and $Z^*_{Ar} = Z^*_D = 1$, from our MD (Fig. 16) we get $\ln\bar{\Lambda} \approx 2.1$, which is in a good agreement ($\sim 10\%$) with Daligault model.

VI. SUMMARY

This Article has focused on the species diffusivity of dense plasma mixtures where one component is moderately weakly coupled and the other component is moderately strongly coupled. We have used classical MD simulations based on the Yukawa interaction for D-Ar mixtures in the temperature range 100–500 eV and at the number density of 10^{25}/cc. MD does not rely on a small-angle scattering approximation, and it does not suffer from ill-defined Coulomb logarithms. The Maxwell-Stefan diffusivity has been calculated using a Green-Kubo relation. In comparing the MS diffusivity to simple combinations of the D and Ar self-diffusivities in the mixture as given by the Darken relation and the common force model, we found that both of the simple models over-predicted the diffusivity. The common force model was in better agreement, but even it was off by a factor of 2 as the Ar mole fraction goes to zero. The discrepancy grows as Z^*_{Ar} is reduced, keeping the argon mass fixed. The failure of these simple models is due to cross-correlations in the D and Ar motion.

We have also compared the Maxwell-Stefan diffusivities calculated in MD with predictions from the kinetic theory by Chapman and Cowling [1] and by Paquette et al. [14]. The Paquette model assumes a Yukawa interaction, thus avoiding the usual issues with the Coulomb logarithm. We find that the Paquette model over-predicts the diffusivity as calculated in MD. This again points to the model missing correlation effects. In this case we have compared the diffusivity as a function of Ar mole fraction at fixed temperature (100, 200, and 500 eV) and fixed total number density (10^{25}/cc), in addition to as a function of Z^*_{Ar} at fixed temperature (100 eV), total number density (10^{25}/cc) and mole fraction (0.1). We found that the kinetic model does not provide good agreement even as the Ar charge is reduced, making the plasma more weakly coupled. These calculations have been done in a regime where the generalized Coulomb logarithm is small (< 2), so it is not surprising that the kinetic theory has appreciable error; it is surprising that the agreement does not improve as the charge asymmetry is reduced. Evidently, the mass asymmetry is sufficient to induce correlation effects that are not captured in the kinetic theory. We also observe that the effective $\ln\Lambda$ has a stronger temperature dependence than predicted by Paquette et al. [14]. While not reported here, a comparison with the diffusivity model of Chapman and Cowling [1] gives similar results.

At this point there is no direct experimental data on diffusion in these regimes. Recent experiments have investigated mixing in inertial confinement fusion experiments [87]. In these experiments an inner part of the plastic ablator was made with deuterated plastic. During an implosion, some of the deuterium mixed into the tritium fuel and the resulting DT neutrons could be differentiated from the TT and DD neutrons by their energy, and thus provided a measure of mixing. This mixing includes diffusion and advected mixing due to Rayleigh-Taylor instability and possibly other hydrodynamic processes. The results of the experiment were compared modeling of the Rayleigh-Taylor instability seeded by the roughness on the exterior of the ablator, using a standard diffusion model. The nature of laboratory experiments that reach hot dense plasma conditions is such that hydrodynamic processes are ubiquitous. Direct measures of mixing include both advection and diffusion, and the data are integrated, relying on models distinguishing the two contributions. In dense fluids at more modest temperatures, it is possible to use scattering techniques to measure the self-diffusivity directly, since the scattering probes the velocity autocorrelation function [88]. Such an experiment for plasma is challenging at the very least. Until a direct experiment is formulated and carried out, integrated experiments and the combination of theory and modeling will provide the only guidance for species diffusion in plasma. Classical MD simulations such as those reported here provide a means to calculate transport coefficients under moderate and strongly coupled conditions. As we have seen in this study, the results of these calculations provide an interesting test of existing models, and there is much more to be learned.

ACKNOWLEDGMENTS

The authors gratefully acknowledge fruitful discussions with John Castor, Kyle Caspersen, Jeff Greenough, A. Bruce Langdon, Paul Miller and Heather Whitley. We also thank Michael Murillo for use of his average atom Thomas-Fermi code for the ionization level in mixture, as well as Phil Sterne for his detailed table of Thomas-Fermi results. TH acknowledges helpful discussions with Jérôme Daligault and Prof. Mark Asta at the initial stage of this work. This work was performed under the auspices of the U.S. Department of Energy by Lawrence Livermore National Laboratory under Contract DE-AC52-07NA27344. The work was funded by the Laboratory Directed Research and Development Program at LLNL under project tracking codes 12-SI-005 and 10-ERD-004. We gratefully acknowledge supercomputer resources provided through the Institutional Computing Grand Challenge Program at LLNL.

[1] S. Chapman and T. Cowling, *The Mathematical Theory of Non-uniform Gases: An Account of the Kinetic Theory of Viscosity, Thermal Conduction and Diffusion in Gases*, Cambridge Mathematical Library (Cambridge University Press, 1939).

[2] J. P. Hansen, E. L. Pollock, and I. R. McDonald, Phys. Rev. Lett. **32**, 277 (1974).

[3] H. Ohta and S. Hamaguchi, Physics of Plasmas **7**, 4506 (2000).

[4] J. Daligault, Phys. Rev. Lett. **108**, 225004 (2012).

[5] J. Daligault, Phys. Rev. E **86**, 047401 (2012).

[6] S. D. Baalrud and J. Daligault, Phys. Rev. Lett. **110**, 235001 (2013).

[7] F. R. Graziani, V. S. Batista, L. X. Benedict, J. I. Castor, H. Chen, S. N. Chen, C. A. Fichtl, J. N. Glosli, P. E. Grabowski, A. T. Graf, S. P. Hau-Riege, A. U. Hazi, S. A. Khairallah, L. Krauss, A. B. Langdon, R. A. London, A. Markmann, M. S. Murillo, D. F. Richards, H. A. Scott, R. Shepherd, L. G. Stanton, F. H. Streitz, M. P. Surh, J. C. Weisheit, and H. D. Whitley, High Energy Density Physics **8**, 105 (2012).

[8] J. P. Hansen and I. R. McDonald, Phys. Rev. Lett. **41**, 1379 (1978).

[9] J. P. Hansen, F. Joly, and I. R. McDonald, Physica **132A**, 4722 (1985).

[10] D. B. Boercker and E. L. Pollock, Phys. Rev. A **36**, 1779 (1987).

[11] G. Salin and D. Gilles, Journal of Physics A: Mathematical and General **39**, 4517 (2006).

[12] L. X. Benedict, M. P. Surh, J. I. Castor, S. A. Khairallah, H. D. Whitley, D. F. Richards, J. N. Glosli, M. S. Murillo, C. R. Scullard, P. E. Grabowski, D. Michta, and F. R. Graziani, Phys. Rev. E **86**, 046406 (2012).

[13] P. E. Grabowski, M. P. Surh, D. F. Richards, F. R. Graziani, and M. S. Murillo, Phys. Rev. Lett. **111**, 215002 (2013).

[14] C. Paquette, C. Pelletier, G. Fontaine, and G. Michaud, The Astrophysical Journal Supplement Series **61**, 177 (1986).

[15] L. Suttorp, Physica A: Statistical Mechanics and its Applications **104**, 25 (1980).

[16] S. Bastea, Phys. Rev. E **71**, 056405 (2005).

[17] C. Alcock and A. Illarionov, The Astrophysical Journal **235**, 534 (1980).

[18] J. Hughto, A. S. Schneider, C. J. Horowitz, and D. K. Berry, Phys. Rev. E **82**, 066401 (2010).

[19] M. V. Beznogov and D. G. Yakovlev, Phys. Rev. Lett. **111**, 161101 (2013).

[20] J. Lindl, Phys. Plasmas **2**, 3933 (1995).

[21] P. Amendt, J. D. Colvin, R. E. Tipton, D. E. Hinkel, M. J. Edwards, O. L. Landen, J. D. Ramshaw, L. J. Suter, W. S. Varnum, and R. G. Watt, Physics of Plasmas **9**, 2221 (2002).

[22] S. Hamaguchi and R. T. Farouki, J. Chem. Phys. **101**, 9876 (1994).

[23] R. T. Farouki and S. Hamaguchi, J. Chem. Phys. **101**, 9885 (1994).

[24] S. Hamaguchi, R. T. Farouki, and H. E. Dubin, J. Chem. Phys. **105**, 7641 (1996).

[25] R. Farouki and S. Hamaguchi, Journal of Computational Physics **115**, 276 (1994).

[26] J. P. Hansen, I. R. McDonald, and E. L. Pollock, Phys. Rev. A **11**, 1025 (1975).

[27] J. D. Kress, J. S. Cohen, D. A. Horner, F. Lambert, and L. A. Collins, Phys. Rev. E **82**, 036404 (2010).

[28] J. Kress, J. S. Cohen, D. Kilcrease, D. Horner, and L. Collins, High Energy Density Physics **7**, 155 (2011).

[29] F. Lambert, J. Clérouin, S. Mazevet, and D. Gilles, Contributions to Plasma Physics **47**, 272 (2007).

[30] E. E. Salpeter, Australian. Journal of Physics **7**, 373 (1954).

[31] J. P. Hansen, G. M. Torrie, and P. Vieillefosse, Phys. Rev. A **16**, 2153 (1977).

[32] Y. Rosenfeld, Phys. Rev. E **47**, 2676 (1993).

[33] Y. Rosenfeld, E. Nardi, and Z. Zinamon, Phys. Rev. Lett. **75**, 2490 (1995).

[34] N. Ashcroft and N. Mermin, *Solid state physics*, Science: Physics (Saunders College, 1976).

[35] B. Firey and N. W. Ashcroft, Phys. Rev. A **15**, 2072 (1977).

[36] K. Wünsch, J. Vorberger, and D. O. Gericke, Phys. Rev. E **79**, 010201 (2009).

[37] D. Gilles, F. Lambert, J. Clérouin, and G. Salin, High Energy Density Physics **3**, 95 (2007).

[38] D. Léger and C. Deutsch, Phys. Rev. A **37**, 4916 (1988).

[39] D. Léger and C. Deutsch, Phys. Rev. A **37**, 4930 (1988).

[40] W. Hubbard and H. DeWitt, The Astrophysical Journal **290**, 388 (1985).

[41] S. Itchimaru, *Statistical Plasma Physics*(Addison-Wesley, Reading, MA, 1991) (1991).

[42] G. Gregori, S. H. Glenzer, W. Rozmus, R. W. Lee, and O. L. Landen, Phys. Rev. E **67**, 026412 (2003).

[43] M. S. Murillo, Phys. Rev. E **81**, 036403 (2010).

[44] L. Landau and E. Lifshitz, *Fluid Mechanics* (Pergamon Press. London, 1963).

[45] J. Hansen and I. McDonald, *Theory of Simple Liquids* (Elsevier Science, 2006).

[46] R. Bird, W. Stewart, and E. Lightfoot, *Transport Phe-*

nomena, Wiley International edition (Wiley, 2007).
[47] R. E. Rudd, W. H. Cabot, K. J. Caspersen, J. A. Greenough, D. F. Richards, F. H. Streitz, and P. L. Miller, Phys. Rev. E **85**, 031202 (2012).
[48] T. Haxhimali and R. E. Rudd, in *Frontiers and Challenges in Warm Dense Matter*, Lecture Notes in Computational Science and Engineering, Vol. 96, edited by F. Graziani, M. P. Desjarlais, R. Redmer, and S. B. Trickey (Springer International Publishing, 2014) pp. 235–263.
[49] S. Groot and P. Mazur, *Non-equilibrium thermodynamics* (North-Holland, 1962).
[50] G. Kagan and X.-Z. Tang, Phys. Plasma **19**, 082709 (2012).
[51] P. Amendt, O. L. Landen, H. F. Robey, C. K. Li, and R. D. Petrasso, Phys. Rev. Lett. **105**, 115005 (2010).
[52] P. Amendt, S. Wilks, C. Bellei, C. K. Li, and R. D. Petrasso, Phys. Plasma **18**, 056308 (2011).
[53] N. March and M. Tosi, *Atomic Dynamics in Liquids*, Dover Books on Physics and Chemistry (DOVER PUBN Incorporated, 1991).
[54] D. McQuarrie, *Statistical Mechanics* (University Science Books, 2000).
[55] J. Horbach, S. K. Das, A. Griesche, M.-P. Macht, G. Frohberg, and A. Meyer, Phys. Rev. B **75**, 174304 (2007).
[56] J. Trullàs and J. A. Padró, Phys. Rev. E **50**, 1162 (1994).
[57] J. Daligault, Phys. Rev. Lett. **96**, 065003 (2006).
[58] A. Einstein, Annalen der Physik **322**, 549 (1905).
[59] R. Kubo, Journal of the Physical Society of Japan **12**, 570 (1957).
[60] R. Kubo, M. Yokota, and S. Nakajima, Journal of the Physical Society of Japan **12**, 1203 (1957).
[61] R. Zwanzig, J. Chem. Phys. **40**, 2527 (1964).
[62] R. Zwanzig, Annual Review of Physical Chemistry **16**, 67 (1965).
[63] Y. Zhou and G. H. Miller, Phys. Rev. E **53**, 1587 (1996).
[64] A. B. Bhatia and D. E. Thornton, Phys. Rev. B **2**, 3004 (1970).
[65] J. G. Kirkwood and F. P. Buff, J. Chem. Phys. **19**, 774 (1951).
[66] D. Frenkel and B. Smit, *Understanding Molecular Simulation: From Algorithms to Applications*, Computational science (Elsevier Science, 2001).
[67] G. Ciccotti, D. Frenkel, and I. McDonald, *Simulation of liquids and solids: molecular dynamics and Monte Carlo methods in statistical mechanics*, North-Holland personal library (North-Holland, 1987).
[68] P. Debye and E. Hückel, Phys. Z **24**, 185 (1923).
[69] M. S. Murillo, High Energy Density Physics **4**, 49 (2008).
[70] All MD simulations made use of the LAMMPS code described by S. J. Plimpton, J. Comput. Phys. 117, 1 1995; http:// lammps.sandia.gov/index.html.
[71] S. Nosé, J. Chem. Phys. **81**, 511 (1984).
[72] W. G. Hoover, Phys. Rev. A **31**, 1695 (1985).
[73] B. J. Alder and T. E. Wainwright, Phys. Rev. A **1**, 18 (1970).
[74] R. P. Feynman, N. Metropolis, and E. Teller, Phys. Rev. **75**, 1561 (1949).
[75] P. Sterne, S. Hansen, B. Wilson, and W. Isaacs, High Energy Density Physics **3**, 278 (2007).
[76] M. S. Murillo, J. Weisheit, S. B. Hansen, and M. W. C. Dharma-wardana, Phys. Rev. E **87**, 063113 (2013).
[77] D. Ofer, E. Nardi, and Y. Rosenfeld, Phys. Rev. A **38**, 5801 (1988).
[78] R. M. More, K. H. Warren, D. A. Young, and G. B. Zimmerman, Physics of Fluids (1958-1988) **31** (1988).
[79] L. S. Darken, Trans. AIME **175**, 184 (1948).
[80] D. C. Douglass and H. L. Frisch, J. Phys. Chem. **73**, 3039 (1969).
[81] M. Shimoji, *Liquid Metals* (Academic Press, London, 1977).
[82] J. P. Hansen and I. R. McDonald, Phys. Rev. A **11**, 2111 (1975).
[83] L. Landau and L. Pitaevskii, *Physical Kinetics* (Pergamon Press. London, 1981).
[84] S. Ichimaru, S. Tanaka, and H. Iyetomi, Phys. Rev. A **29**, 2033 (1984).
[85] D. O. Gericke, M. S. Murillo, and M. Schlanges, Phys. Rev. E **65**, 036418 (2002).
[86] G. Salin and J.-M. Caillol, Physics of Plasmas **10**, 1220 (2003).
[87] V. Smalyuk, R. Tipton, J. Pino, D. Casey, G. Grim, B. Remington, D. Rowley, S. Weber, M. Barrios, L. Benedetti, D. Bleuel, D. Bradley, J. Caggiano, D. Callahan, C. Cerjan, D. Clark, D. Edgell, M. Edwards, J. Frenje, M. Gatu-Johnson, V. Glebov, S. Glenn, S. Haan, A. Hamza, R. Hatarik, W. Hsing, N. Izumi, S. Khan, J. Kilkenny, J. Kline, J. Knauer, O. Landen, T. Ma, J. McNaney, M. Mintz, A. Moore, A. Nikroo, A. Pak, T. Parham, R. Petrasso, D. Sayre, M. Schneider, R. Tommasini, R. Town, K. Widmann, D. Wilson, and C. Yeamans, Phys. Rev. Lett. **112**, 025002 (2014).
[88] A. Meyer, Phys. Rev. B **81**, 012102 (2010).